JOURNAL OF GEOPHYSICAL RESEARCH, VOL. 103, NO. B11, PAGES 27,465–27,487, NOVEMBER 10, 1998

Flow and convective cooling in lava tubes

S. E. H. Sakimoto[1]

NASA Goddard Space Flight Center, Geodynamics Branch, Greenbelt, Maryland

M. T. Zuber[2]

Department of Earth, Atmospheric, and Planetary Sciences, Massachusetts Institute of Technology, Cambridge

Abstract. Tube-fed basaltic lava flows with lengths ranging from 10 to 200 km are inferred to exhibit similar amounts of cooling. To explain the wide range of implied cooling rates, we consider forced convection as a dominant cooling process in lava tubes and present solutions that express mean temperature versus distance down the tube as a function of flow rate and flow cross section. Our models treat forced convective thermal losses in steady laminar flow through a lava tube with constant temperature walls and constant material properties. We explore the effects of different wall temperature and heat flux rate boundary conditions for circular tube and parallel plate flows over a range of tube sizes, plate spacings, eruption temperatures, and volume flow rates. Results show that nonlinear cooling rates over distance are characteristic of constant wall temperature for a piecewise parallel plate/circular tube model. This provides the best fit to temperature observations for Hawaiian tubes. Such a model may also provide an explanation for the very low (~10°C) cooling observed in ~10 km long Hawaii tube flows and inferred in longer ~50 to 150 km tube-fed flows in Queensland. The forced convective cooling model may also explain similar flow morphologies for long tube-fed basaltic lava flows in a wide variety of locations, since small variations in eruption temperature or flow rate can accommodate the entire range of flow lengths and cooling rates considered. Our results are consistent with previous suggestions that long basaltic flows may be a reflection of low slopes, a particularly steady moderate eruption rate, and well-insulated flow, rather than of high discharge rates.

1. Introduction

Lava tubes are a primary mode of lava emplacement in basaltic volcanism and have fed many of the longest lava flows [*Malin,* 1980], as well as contributing substantially to resurfacing of basaltic shield and plains volcanism terrains [e.g., *Greeley*, 1987; *Holcomb*, 1987; *Hon et al.,* 1994]. In addition, tube flows are responsible for feeding extensive inflated sheet flows in Hawaii [e.g., *Hon et al.,* 1994; *Kauahikaua,* 1996], and they have played an important role in the emplacement of the Columbia River Basalts [*Self et al.,* 1996] and other flows. The longest recognized subaerial flows on Earth [e.g., *Atkinson et al.,* 1975] as well as the longest North American basaltic flows (outside of the Columbia River Basalts) are though to be tube or tube-fed flows. These include the long (> 50 km) Carey and Grassy Cone flows of the Craters of the Moon lava field [*Kuntz et al.,* 1982, 1992], the 60 km long Shoshone lava field [*Kuntz et al.* 1992] on the Snake River Plain, the New Mexico 60 km McCartys flow and 90 km Fence Lake flow in the Zuni-Bandera field [*Theilig,* 1990a], the 42 km long Lucero field [*Baldridge,* 1990], and the >70 km long Carrizozo field [*Theilig,* 1990b; *Keszthelyi,* 1995], as well as the 46 km Indian Heaven flow field in Oregon [*Hammond,* 1990]. The collapse pit chains characteristic of drained lava tubes are common on Hawaiian volcanoes, Medicine Lake volcano in California [*Waters et al.,* 1990; *Donnelly-Nolan,* 1992], within the Snake River Plains basalt flows [*Greeley,* 1977, 1982], and in near-vent Undara volcano flows [e.g., *Atkinson et al.,* 1975]. Morphologically similar features have been reported in association with volcanic flows on Mars and Venus [e.g., *Carr,* 1981; *Hodges and Moore,* 1992; *Head et al.,* 1992]. On low slopes, lava tubes are unlikely to drain and leave caves and collapse pit chains, but evidence for flow inflation, the presence of minimal cooling over the flow length, and an apparent concentration of flow within the interior relative to the exterior often can indicate the presence of a tube or tube network that fed a lava flow [*Cashman et al.,* 1993; *Hon et al.,* 1994; *Cashman et al.,* 1994; *Kauahikaua,* 1996].

Lava tube flow temperature measurements contain information on the nature of the cooling processes that operate within the tube. Different temperature distributions are predicted for constant or variable heat flux rates along the tube as well as thermal mixing or boundary layer formation within the flowing lava. Measurements of cooling rate with distance from the vent will help to identify the relative importance of different cooling processes, as will the knowledge of the temperature distributions across the flow, along the flow, and at the wall/lava boundary.

Previous data for lava tube temperatures include a handful of papers where the total temperature drop along the tube is reported [e.g., *Swanson*, 1973; *Helz et al.*, 1991], and prior

[1]Now at Universities Space Research Association at the Geodynamics Branch, NASA Goddard Space Flight Center, Greenbelt, Maryland.

[2]Also at Laboratory for Terrestrial Physics, NASA Goddard Space Flight Center, Greenbelt, Maryland.

Paper number 97JB03108.
0148-0227/98/97JB-03108$09.00

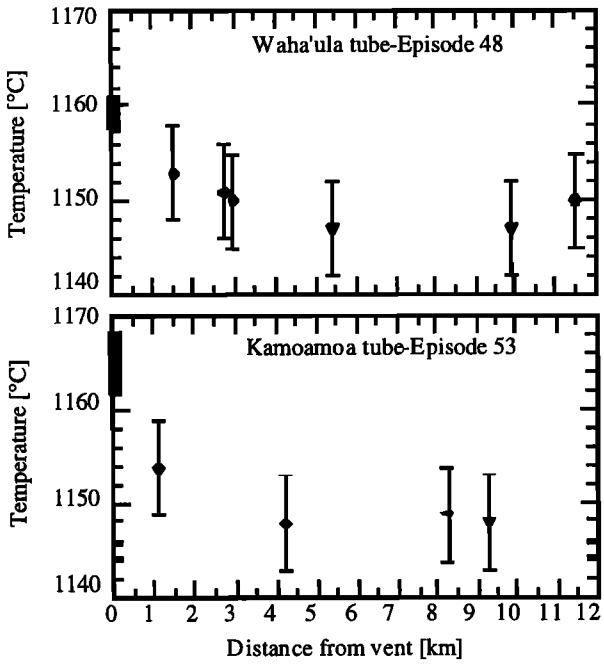

Figure 1. Temperature data for lava tube samples for the Waha'ula and Kamoamoa tubes [*Cashman et al.*, 1994, Tables 1 and 2]. Absolute temperature error bars are ±5°C, but relative errors are less. Diamonds indicate samples from tube skylights, triangles indicate breakout samples, and circles indicate samples from coastal spatter at the tube exit. Solid bars are eruption temperatures from *Helz et al.* [1991].

knowledge of the cooling rates and modeling efforts primarily tried to match the approximately 10°C drop over 10 km previously noted for Hawaiian East Rift Zone flows [*Swanson*, 1973; *Helz et al.*, 1991; *Keszthelyi*, 1995]. More recent data (C. Thornber, personal communication, 1997) shows a wider range of cooling rates (0.5° to 1°C/km), and *Cashman et al.* [1994, Tables 1 and 2] includes lava tube temperatures based on the *Helz and Thornber* [1987] glass geothermometry method for samples from skylights, breakouts, and ocean-entry tube spatter. Figure 1 is a plot of the *Cashman et al.* [1994] temperature data as a function of distance down the tube. The data are for the Waha'ula tube Episode 48 eruption from the Kupaianaha vent and the Kamoamoa tube Episode 53 eruption from the Pu'u 'O'o vent. The error bars on the temperatures are ±5°C, but the relative temperatures are consistent since there are no MgO content reversals (K.V. Cashman, personal communication, 1997). *Helz et al.* [1991] reported glass geothermometry eruption temperatures for the Kupaianaha vent of 1158–1161°C, which includes Episode 53. The Pu'u 'O'o eruption temperatures reported by *Helz et al.* do not include Episode 48 and are assumed to be 1162–1168° as in previous Pu'u 'O'o Episodes [*Helz et al.*, 1991]. The data in Figure 1 show that the highest cooling rates are near the tube entrances, as would be expected for a predominantly convective cooling regime, where the wall temperature has stabilized to a constant temperature [*Sakimoto and Zuber*, 1996]. Tube cooling models that consider constant heat flux rates over the tubes or tube segments (e.g., *Keszthelyi* [1995] and the constant heat flux models of this study) result in a linear or piecewise linear decrease of temperature over distance that is dependent on slope and tube size rather than flow rate and aspect ratio. While *Keszthelyi*'s [1995] models are compatible with the approximately 1°C/km cooling noted above, the predicted linear cooling rates are not compatible with observed nonlinear cooling rates [*Cashman et al.*, 1994] (Figure 1) or for explaining the lengths of much longer terrestrial tube flows that have been emplaced in seemingly similar circumstances.

This study considers several convective cooling models that predict thermal losses in steady, hydrodynamically developed, thermally developing laminar flow through a lava tube with either constant temperature walls or constant heat flux at the walls for a flow with constant material properties. We explore the effects of different wall temperatures or heat flux rates for circular tube and parallel plate flows over a range of tube sizes, plate spacing, eruption temperatures, and volume flow rates. Since the recent temperature data are the result of glass geothermometry analysis of tube samples, we have shown the model results in terms of mean bulk temperature versus distance so that the differences in cooling rates over distance are apparent and can be plotted with the temperature data. The mean bulk temperature is used since the glass geothermometry sampling technique often consists of dropping a cable into the tube flow at a skylight and pulling back out the cable and the lava that has collected around the sampling end of the cable. This will tend to produce a sample that is somewhat mixed since it passes through the boundary layer, into the flow center, and back through the boundary layer with probable accretion of the flow material onto the sample throughout the process. Some of the variations in the data in Figure 1 will be due to the sample retrieval techniques, rather than to the sample analyses techniques, since the retrieval methods are likely to be sampling a slightly different version of the thermal cross section at each location and retrieval.

2. Approach

2.1. Assumptions

We assume incompressible laminar flow throughout this analysis. This assumption is observation-driven, since we have no documented cases of fully turbulent lava flow. For circular cross sections and smooth pipes, the flow becomes unstable at $Re = 2000$ and fully turbulent at $Re = 4000$ [e.g., *White*, 1991]. Figure 2 shows Re as a function of tube radius, flow viscosity, and flow rate. At these tube sizes and moderate flow rates, the flow is expected to be laminar. However, it should be noted that for thermal reasons discussed later, we have approximated a partially filled tube as a parallel plate flow but that for this geometry, the critical Reynolds number is 500 [e.g., *Chow*, 1959]. Consequently, the thermal models given here will not be appropriate for channel-type flows for larger Re. This may make a difference for some large flows in partially full tubes. Incompressible flow is an important simplifying assumption, although there is evidence for changes in vesicularity along the path of the flow [*Swanson and Fabbi*, 1973; *Cashman et al.*, 1994].

The flow is assumed to be Newtonian, hydrodynamically developed, and thermally developing, so that the velocity profile is parabolic and the thermal boundary layer is growing. For laminar flow, it will take at most 100 diameters to establish and develop the velocity boundary layer and a parabolic velocity profile [see *White*, 1991] and substantially less for most lava tubes [*Sakimoto et al.*, 1997]. However, basalt is not particularly conductive, so the thermal boundary layer grows very slowly and the thermal entry length is very

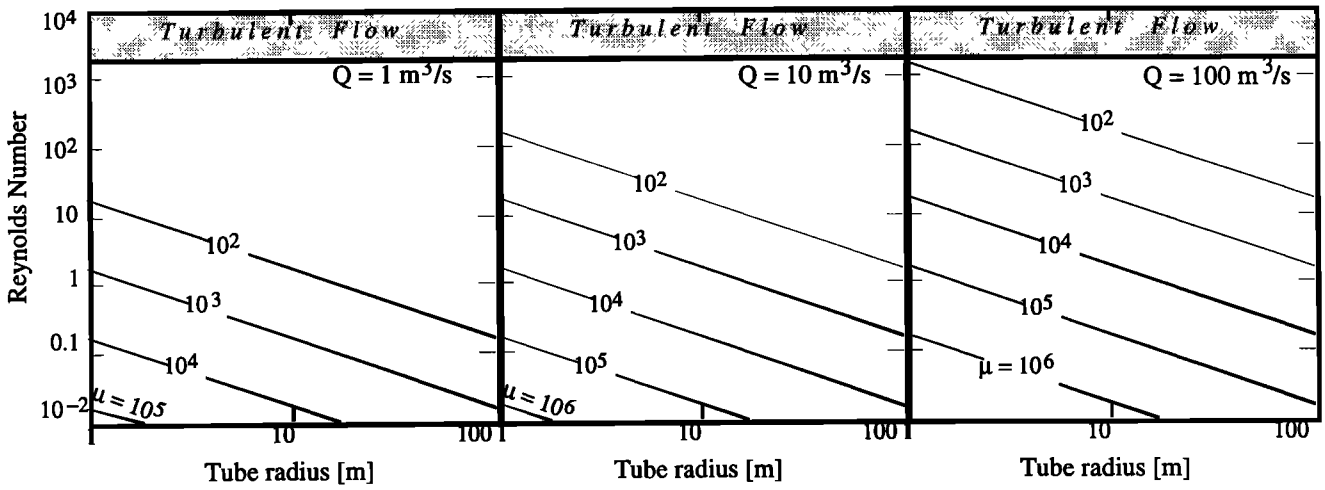

Figure 2. Reynolds number *(Re)* versus lava tube radius for flow rates of 1, 10, and 100 m^3/s. Contours are in viscosity in Pa s, and the transitional and turbulent flow regimes are shaded. For moderate flow rates and basaltic viscosities, the flows are within the laminar regime.

long. For example, using the thermal entrance length expression in Table 1, as well as the laminar flow, and heat capacity and thermal conductivity values in Table 1, the thermal entrance length in tube diameters is 46 $Re\mu$ or, for laminar flow, up to 92,300μ, where μ is the dynamic viscosity in Pa s So, for a viscosity of 1000 Pa s, and a tube diameter of 1 m, the thermal entry length for $1<Re<2000$ would be between 46 km and 92,000 km, which ensures that we are always dealing with thermally developing flow. Physically, this yields a hot flow center with a constant temperature flow center through the thermal entrance length ($dT/dz = 0$ at $r = 0$) and a thermal boundary layer that grows as a function of distance down the tube. If the flow is still within the hydrodynamic entrance length, there can be up to 10% error in flow rates due to applying the driving force flow calculation to partially developed flow [*Sakimoto et al.*, 1997]. Since the thermal solutions are moderately sensitive to flow rate variations, this error can affect the predicted temperatures but is not likely to change the model results within the current error bars of available temperature measurements.

Steady flow is assumed, since tube formation is most likely in eruptions with steady eruption rates and durations of more than a few days [e.g., *Peterson et al.*, 1994]. Additionally, the boundary between the fluid and the tube wall is assumed to be no slip, since observed tube flows often have a noticeable velocity gradient between the tube center and the tube wall.

In a full lava tube in thermally undeveloped flow, the temperature is at a maximum at the tube center and decreases radially outward to the walls. Both the circular tube and the parallel plate convective cooling models used here assume either a constant wall temperature or a constant wall heat flux. For the constant temperature boundary condition, we have assumed that the tube wall location will reach an equilibrium at a constant temperature T_w and that T_w is 1077°C, the temperature at which Kilauea basaltic lava is approximately 55% crystallized [cf. *Marsh*, 1981]. Since T_w varies with composition, it should be adjusted to reflect any available crystallinity versus temperature data if this model is used on other flows. At $T \leq T_w$ the lava has a sufficient interlocking crystalline network to behave as a brittle solid and thus cannot be incorporated into the flow by shear forces from the flowing lava. If the temperature at the wall increases above this significantly, the wall will become less viscous and susceptible to thermomechanical erosion, and if the temperature decreases significantly, either the heat flux from the flow will reheat it or the wall location will migrate inwards toward the tube center. This 55% crystallinity temperature (or something similar) seems a reasonable assumption for tubes that develop as a flow concentration within a large sheet flow [e.g., *Hon et al.*, 1994], where the wall temperature should be that of the material that has cooled and is too viscous to flow easily. It should also be reasonable for long-lived tubes that

Table 1. Parameters, Notation, Assumed Values, and Units

Parameter	Notation	Value[a]	Units
Tube radius	a		m
Tube diameter	D	$2a$	m
Plate spacing	$2d$		m
Flow width	w		m
Radial coordinate for tube flows	r		m
Height coordinate for parallel plate flows	y		m
Length coordinate for tube and plate flows	z		m
Characteristic dimension	D_c	D or $2d$	m
Cross-section area	A	πa^2 or $2dw$	m^2
Wetted perimeter	P	πD or $2w$ for $w>>d$	
Hydraulic diameter	D_h	$D_h = 4A/P$	m
Density	ρ	2600	kg m^{-3}
Thermal conductivity	k	1.3	J m^{-1} s^{-1} K^{-1}
Specific heat capacity	C_p	1200	J kg^{-1} K^{-1}
Entrance temperature	T_e		°C
Wall temperature	T_w		°C
Mean bulk fluid temperature	T_m		°C
Wall heat flux	q_w		Wm^{-2}
Hydrodynamic entrance length	L_{he}	$0.05DRe$	m
Thermal entrance length	L_{te}	$0.05RePrD$	m

[a] If no value is assigned, parameter is different for each tube and/or solution (see Table 3).

have heated the surrounding rock or tubes that are thermomechanically eroding their base and/or walls. For small tubes or low flow rates, the shear forces from the flow may not be large, and T_w could be higher. Numerical simulations with temperature- and shear rate-dependent viscosities suggest that T_w could be as high as 1130°C [*Sakimoto*, 1995b, also, unpublished data, 1997], near the point encountered in cooling where the suspended crystals begin to interact and the viscosity undergoes a large increase. For most cases, we have assumed T_w=1077°C, but several of the models have been evaluated with both T_w =1077° and T_w =1130°C for comparison.

This problem is essentially a conductive cooling problem with conductive heat flow both within the fluid and across the fluid wall interface. The heat flux rates in conductive cooling are functions of the thermal conductivity of the material and of the temperature difference across the zone of heat transfer. Since we have assumed constant properties, and the same thermal conductivity for the fluid and solid basalt, the temperature gradients determine the location of the slowest or limiting heat transfer rate. Within the tube, the difference between the eruption and wall temperatures ranges from 30° to 100°C, while outside the tube, the temperature decreases from the wall temperature of 1077° to ambient surface temperatures of ~30°C. The temperature difference between the tube wall and ambient conditions is then an order of magnitude larger than the temperature difference between the flow center and the tube wall. This suggests that the limiting process in the cooling is the heat transfer within the flow to the tube walls and that any heat transferred to the walls can be conducted (or convected or radiated [see *Keszthelyi*, 1995]) away as fast as it is delivered. The temperature distribution within the tube will then control the cooling of the tube, and external conditions (other than the wall temperature) will have little or no effect. Consequently, the factors that are most important in controlling the internal tube temperature distribution (the flow rate, distance down the tube, and the shape of the cross section of the flow) will control the cooling in this study.

Since we have argued for an equilibrium wall temperature as the most reasonable boundary condition, the constant wall heat flux models are presented primarily for comparison here. We have used a range of wall heat flux values that includes those proposed in previous work [*Hardee*, 1983, 1993; *Realmuto et al.*, 1992; *Keszthelyi*, 1995].

For a full tube, the boundary conditions of a constant wall temperature are clear. For a partially full tube, there is the complication of the tube atmosphere filling the tube cavity. This cavity above the lava will act as a blackbody region with nearly uniform internal temperature of the gas, top surface of the flow, and wall surface. There has not been a quantitative assessment of the effect of heat transport in the void above a partially full tube, and such a study is much needed. For this analysis we assume that the radiative losses of the top flow surface will cool it to a temperature below that of the flow interior. We have assumed that this temperature is equal to T_w, so that the thermal boundaries of the tube flow are symmetrical and, as for the full tube, the flow rate, distance down the tube, and the shape of the cross section of the flow will control cooling. Important considerations thus include the geometry of the cross section as well as flow rate. Rather than present a host of solutions, one for each potential tube geometry, we consider circular tube flow and parallel plate flow, which are straightforward to set up and calculate, and can act as end members for a range of tube geometries. For more accurate work once more detailed temperature and tube geometry data are available, solutions for a variety of cross section geometries are tabulated in the literature [e.g., *Shah and London*, 1978].

Table 2. Dimensionless Parameters

Parameter	Notation	Expression
Dimensionless axial distance	z^*	$\frac{zkA}{\rho C_p Q D_h^2}$ or $\frac{zk}{\rho C_p V D_h^2}$
Dimensionless fluid bulk mean temperature	θ_m	$\frac{T_m - T_e}{T_e - T_w}$
Dimensionless fluid temperature	θ	$\frac{T - T_e}{T_e - T_w}$
Reynolds number	Re	$\frac{\rho U D_h}{\mu}$
Nusselt number	Nu	hD_h/k
Prandtl number	Pr	$\frac{\mu C_p}{k}$
Peclet number	Pe	$RePr$
Local Nusselt number	$Nu_{z,bc}$	$f(z^*)$[a]
Mean Nusselt number	$Nu_{m,bc}$	$f(z^*)$[a]

[a] Nu is a function of dimensionless distance and varies with the flow geometry. The subscript bc is a place holder for the boundary condition.

So, for steady laminar flow in a tube with constant temperature walls, the temperature distributions within the tube are known to be a function of the dimensionless distance down the tube $z^* = z/D_h RePr$ (see *Shah and London* [1978] and Tables 1 and 2 for variable definitions). When we use flow rates for problem input, instead of a mean velocity, the dimensionless distance is $z^* = (zPk)/(4\rho D_c Q C_p)$, where z is the distance from the tube entrance, P is the "wetted perimeter" [cf. *White*, 1991], D_c is a length characteristic of the geometry (e.g., the tube diameter or plate spacing), and Q is the volume flow rate. Since for this study, the thermal conductivity k, flow density ρ, and heat capacity C_p are considered to be constant, cooling is a function of z, P, D_c, and Q. From this it is clear that once we stipulate the flow rate and distance down the tube, the remaining consideration is the geometry in terms of P/D_c. For full, circular, tubes, P/D_c is simply π and we can use the classic circular pipe Grätz type of solution (see the appendix), and there is no diameter dependence in the cooling. This diameter independence is a direct result of defining the model in terms of flow rate instead of average velocity and tube diameter. For other geometries, there will be some type of geometry dependence, and the cooling solution dynamically closest to the problem will be that with the closest P/D_c. The larger the value of P/D_c, the greater the cooling will be relative to the circular tube case.

For example, consider a full rectangular tube with a flow depth of 1 m and a flow width of 3 m. The ratio P/D_c is 8. Using a circular tube solution where $P/D_c = \pi$ is likely to underestimate the cooling, but a parallel plate solution, where $P/D_c = 6$, is a closer match. Numerical simulations confirm that for even this 3:1 aspect ratio, the parallel plate solution accounts for ≈ 80% of the heat lost in the full rectangular solution, whereas the circular tube solution predicts heat losses somewhat less than half the actual losses. As aspect ratios increase, the heat lost through the side walls decreases relative to the heat lost through the top and bottom walls, and the parallel plate solution becomes an increasingly good

approximation. As the aspect ratio approaches 1:1, the heat flow from the constant wall temperature parallel plate solution approaches approximately 2/3 that of a round tube with a diameter equal to the plate spacing. For aspect ratios greater than 10:1, the difference is usually less than 10%. Knowing that the parallel plate solution underestimates the cooling losses, we have compensated somewhat by using the higher estimates of flow aspect ratio where there is a range reported. For flows where we have few or no constraints on the aspect ratio of the flow cross section, we have used the same values as in previous flows to allow a direct comparison of the predicted cooling rates. In general, these model results apply both to the simple shapes assumed as well as to a range of irregular shapes that have equivalent heat loss characteristics (P/D_e, material properties, thermal boundary conditions, and flow rate).

The convective cooling models presented here include the implicit assumption that the flow is not thoroughly mixed after it enters the lava tube. Such a remixing would eradicate the thermal boundary layer, and restart its growth, with commensurably higher cooling losses. If lava within the entire tube is in continuous slow laminar flow, then the assumption is reasonable. However, the presence of large abrupt tube size or slope changes will lead to locally higher cooling losses as the thermal boundary layer is reestablished, and our models will underestimate cooling rates unless they are applied to each section of the tube after remixing. From the agreement of the tube temperature data with the model prediction for the Hawaiian tubes in this study, this appears to be a reasonable assumption. Assuming complete remixing at each of the sections reported for the Waha'ula tube by *Keszthelyi* [1995] resulted in predicted cooling rates that were twice as large as those observed.

We have also assumed that there is no long-term lava-water (or permafrost) interaction of a large enough magnitude to influence the cooling rates. However, if extended interaction between the lava and water was present, as might be the case for a submarine flow, it may be reasonable to use this type of convective cooling model with an adjusted (higher) constant heat flux boundary condition. For the Queensland flows, which were erupted in the dry season, and the Mars flows, which presumably erupted onto a dry surface, this is probably a very good assumption. The effects of cooling by rainfall on the Hawaiian flows are not as clear. *Keszthelyi* [1995] suggests that the effects of rainfall are not insignificant, but the analysis is a simple one that depended primarily on the diameter of the 100°C isotherm surrounding the lava tube. The study predicts that the bigger the isotherm diameter, the more important will be the rainfall effects, and the higher will be the cooling rate. This prediction ignores the significant consideration of the proximity of the isotherm to the lava tube and the implied temperature gradient in the surrounding rock, which strongly influences heat flow.

For our model, conduction in the flow direction is ignored, since the Prandtl number is expected to be much greater than one [e.g., *Bird et al.*, 1960; *Shah and London*, 1978], and heat is convected much faster down flow than it could be conducted in the same direction. The radiative losses are assumed to be insignificant, since the area of skylights, and thus the area exposed to radiative cooling, is very small [*Keszthelyi*, 1995].

Additionally, the material properties (viscosity, density, and thermal conductivity) are assumed to be constant. This is an important simplifying assumption, but it is also made since these models are intended for flows that are well insulated and undergo minimal amounts of cooling, and the temperature-dependent variations in thermal conductivity and heat capacity will be small. The minimal cooling observed in tube flows also prompted the neglect of latent heat of crystallization. The assumption of constant density induces more potential error, since there is some evidence for significant changes in vesicularity along flow paths [*Swanson and Fabbi*, 1973; *Cashman et al.*, 1994]. However, data sets that track both tube flow temperature and the density within the tube over the flow length are scarce, so density variations are neglected for these models. While we know that other property (thermal conductivity, vesicularity, rheology) variations are often present and have measured variations of some of them in a few flows, it is not yet clear what range or property values is appropriate as input for a general cooling model, and this set of models cannot accommodate variations within the flow. Consequently, we have assumed constant values. The next generation of models will most likely need to consider both density variations as well as potential thermal conductivity variations with vesicularity, and may need to consider bubble- or crystal-driven non-Newtonian effects in the velocity profile.

There are two major difference between this study and the other existing thermal model of tube flow [*Keszthelyi*, 1995]. The first difference is the treatment of the heat convected down the tube, which this study explicitly solves for, and Keszthelyi assumes is a uniform process in a well-mixed tube. The second difference is the selection of the rate-limiting process in the heat transfer from the flow interior through tube walls to the surroundings. This study assumes that the rate-limiting process is within the flow boundary layer, and so the form of the external heat transfer processes is not important. Keszthelyi assumes that the rate-limiting process(es) are external to the tube, which is well mixed and without a significant internal thermal boundary layer. When the rate-limiting processes are external to the tube, ambient conditions such as burial depth and rain percolation become important, and results must be calculated for each tube section with different external conditions. For example, when the rate-limiting heat transfer is external to the tube the proximity of the tube to the surface strongly affects the cooling. Figure 3 shows the steady state two-dimensional temperature field for the conductive solution used by *Keszthelyi* [1995]. Here, the isotherms at intervals of 100°C [*Eckert and Drake*, 1987, equations 3-65 and 3-70] have been plotted for a 1-m-diameter tube with a tube center 1.5 m below the surface. This solution is for an isothermal solid source and is commonly used in applications such as finding the temperatures around a buried cable. Using it alone precludes consideration of heat flux differences caused by either radial or axial temperature differences within the tube such as a thermal boundary layer or the cooling along the tube. However, this solution provides information on the effects of a nonuniform thermal gradient around a tube and can be added as a linear correction to a convective solution with a constant flux boundary condition for cases where the limiting heat flow rate in the problem is not within the thermal boundary layer within the flow. For the current study, the burial depth is not a significant factor unless it is very large (e.g., greater than 20 tube diameters or so) and affects the relative size of the external thermal gradient compared to the thermal gradient in the boundary layer.

Tube sizes and average velocities are very poorly known, and the model is sensitive to them, so assuming a range of

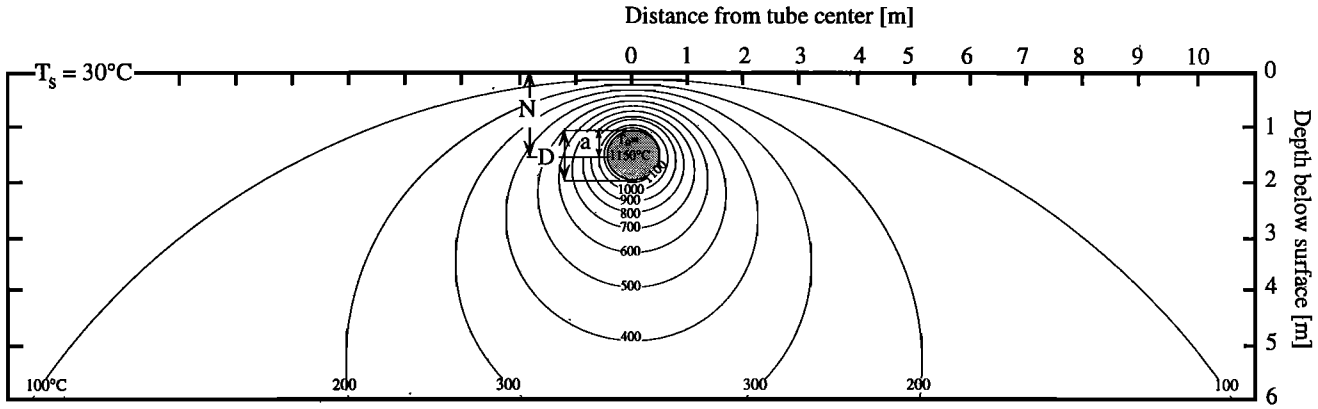

Figure 3. Two-dimensional temperature field for conductive heat flow from an isothermal cylindrical solid in a semi-infinite half space. N is the distance of the cylinder center below the surface, a is the radius, and D is the diameter. The surface is held at temperature T_s, and the cylinder is held at T_0. The plot shows the effects of a nearby free surface on the temperature field and thermal gradients around the cylinder with a constant temperature boundary.

values for both results in very poorly constrained cooling predictions. Flow rates are rather better [e.g., *Kauahikaua et al.*, 1996], so the best constrained results from the cooling models in this study are obtained using observed or inferred flow rates. However, for prehistoric or remotely imaged flows, this is not feasible. For these cases we must estimate reasonable flow rate ranges from the tube dimensions, underlying slopes, and a range of reasonable viscosities. In order to use this approach with these models, the rheological properties must be assumed to be constant both across the tube section and down the tube. For basaltic flows like those considered here, the viscosity can either be based on field measurements [e.g., *Shaw et al.*, 1968] or a temperature-dependent rheology model [e.g., *Shaw et al.*, 1968; *Shaw*, 1969; *Sakimoto*, 1995a]. At the tube entrance temperatures assumed here, all flows start out well in the Newtonian range with respect to crystallinity [*Shaw et al.* 1968; *Shaw*, 1969; *Sakimoto*, 1995a]. For these temperatures and the temperatures these models predict at the tube ends, the non-Newtonian effects are likely to be small. For flows where initial temperatures or cooling effects put the flow within the non-Newtonian range of behavior, the primary effects will be to extend entrance lengths and reduce flow rates. For estimating flow rate and viscosity ranges, the approach of *Sakimoto et al.* [1997] will yield flow rates for pressure-driven, gravity-driven, or combined flow for the Newtonian as well as the power law and Bingham rheologies if tube dimensions and underlying slopes are estimated.

2.2. Analytic Cooling Models

We consider four convective cooling solutions: a circular tube and a parallel plate with constant temperature walls and a circular tube and parallel plate with constant heat flux at the walls. All four solutions assume hydrodynamically developed flow, constant material properties, constant temperature at the entrance, no conduction in the flow direction, and no viscous dissipation. These are all eigenfunction summations that yield solutions for mean tube temperature versus distance down the tube. All four have been checked for accuracy against results in the literature. They are presented in their entirety in the appendix, both for comparison between solutions and since some of the sources are out of print or in journals not normally found in physical volcanology collections.

Consider the similar problems of steady state thermal losses from a hot fluid flowing in a circular tube or between parallel plates. In Cartesian coordinates, the energy equation is

$$V_x\frac{\partial T}{\partial x}+V_y\frac{\partial T}{\partial y}+V_z\frac{\partial T}{\partial z}=\frac{k}{\rho C_p}\left[\frac{\partial^2 T}{\partial x^2}+\frac{\partial^2 T}{\partial y^2}+\frac{\partial^2 T}{\partial z^2}\right]. \quad (1)$$

where T is the temperature, k is the thermal conductivity, C_p is the heat capacity, ρ is the flow density (see Table 1), and V_x, V_y, and V_z are the velocity components. For flow in a round tube with the coordinate system of Figure 4a and axial symmetry, equation (1) becomes

$$V\frac{\rho C_p}{k}\frac{\partial T}{\partial z}=\frac{1}{r}\frac{\partial}{\partial r}\left(r\frac{\partial T}{\partial r}\right)+\frac{\partial^2 T}{\partial z^2}. \quad (2)$$

In laminar flow the last term on the right is very small compared to the other terms and so is normally neglected. Equation (2) may be rewritten as

$$V_z\frac{\partial T}{\partial z}=\frac{k}{\rho C_p}\left[\frac{\partial^2 T}{\partial r^2}+\frac{1}{r}\frac{\partial T}{\partial r}\right]. \quad (3a)$$

For equation (3a), we will consider either a constant wall temperature set of boundary conditions

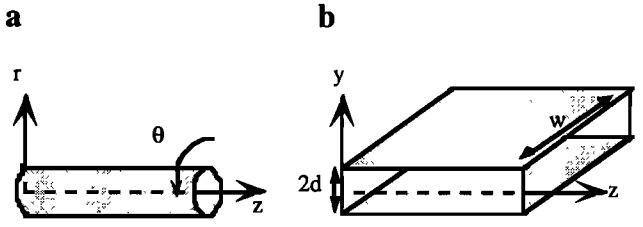

Figure 4. (a) Cylindrical coordinate system used for tube flow problem. Flow is in positive z direction and axisymmetric in θ if tube is full and boundary conditions are axisymmetric in θ. (b) Parallel plate coordinate system. Flow is in positive z-direction with identical boundary conditions on the upper and lower walls, with width $w>d$, where d is the half-separation distance of the plate.

$$\begin{array}{lll} T = T_e & r \le a & -\infty \le z < 0 \\ T = T_w & r = a & 0 < z \le +\infty \\ \partial T/\partial z = 0 & r = 0 & -\infty \le z \le +\infty \\ T = T_w & 0 \le r \le a & z = +\infty \end{array} \quad (3b)$$

where T_e is the constant entrance temperature, T_w is the constant wall temperature, and a is the tube radius, or a constant wall heat flux set of boundary conditions

$$\begin{array}{lll} T = T_e & r \le a & -\infty \le z < 0 \\ \partial T/\partial r = q_w a/k & r = a & 0 < z \le +\infty \\ \partial T/\partial z = 0 & r = 0 & -\infty \le z \le +\infty \\ T = T_w & 0 \le r \le a & z = +\infty \end{array} \quad (3c)$$

where q_w is a specified constant wall heat flux.

For unidirectional flow between parallel plates with the coordinate system of Figure 4b, equation (1) becomes

$$V_z \frac{\partial T}{\partial z} = \frac{\rho C_p}{k} \frac{\partial^2 T}{\partial y^2}. \quad (4a)$$

For equation (4a) we will consider either a constant wall temperature set of boundary conditions

$$\begin{array}{lll} T = T_e & y \le d & -\infty \le z < 0 \\ T = T_w & y = d & 0 < z \le +\infty \\ \partial T/\partial z = 0 & y = 0 & -\infty \le z \le +\infty \\ T = T_w & 0 \le y \le d & z = +\infty \end{array} \quad (4b)$$

where $2d$ is the plate spacing, or a constant wall heat flux set of boundary conditions

$$\begin{array}{lll} T = T_e & y \le d & -\infty \le z < 0 \\ \partial T/\partial y = q_w a/k & y = d & 0 < z \le +\infty \\ \partial T/\partial z = 0 & y = 0 & -\infty \le z \le +\infty \\ T = T_w & 0 \le y \le d & z = +\infty \end{array} \quad (4c)$$

Figure 5 shows a comparison of the constant temperature wall solutions for circular tube (equations (3a) and (3b)) and parallel plate (equations (4a) and (4b)) flows with widths equal to 12 times the plate spacing. Dimensionless fluid bulk mean temperature $[(T_m-T_e)/(T_e-T_w)]$ is plotted versus distance from the tube entrance and volume flow rate. The assumed values for k, C_p and ρ are from Table 1. From Figure 5, it is clear that the circular tube flows are more thermally efficient. The tube flows need approximately one-tenth the flow rate of the parallel plate flows to maintain the same drop in mean tube temperature with

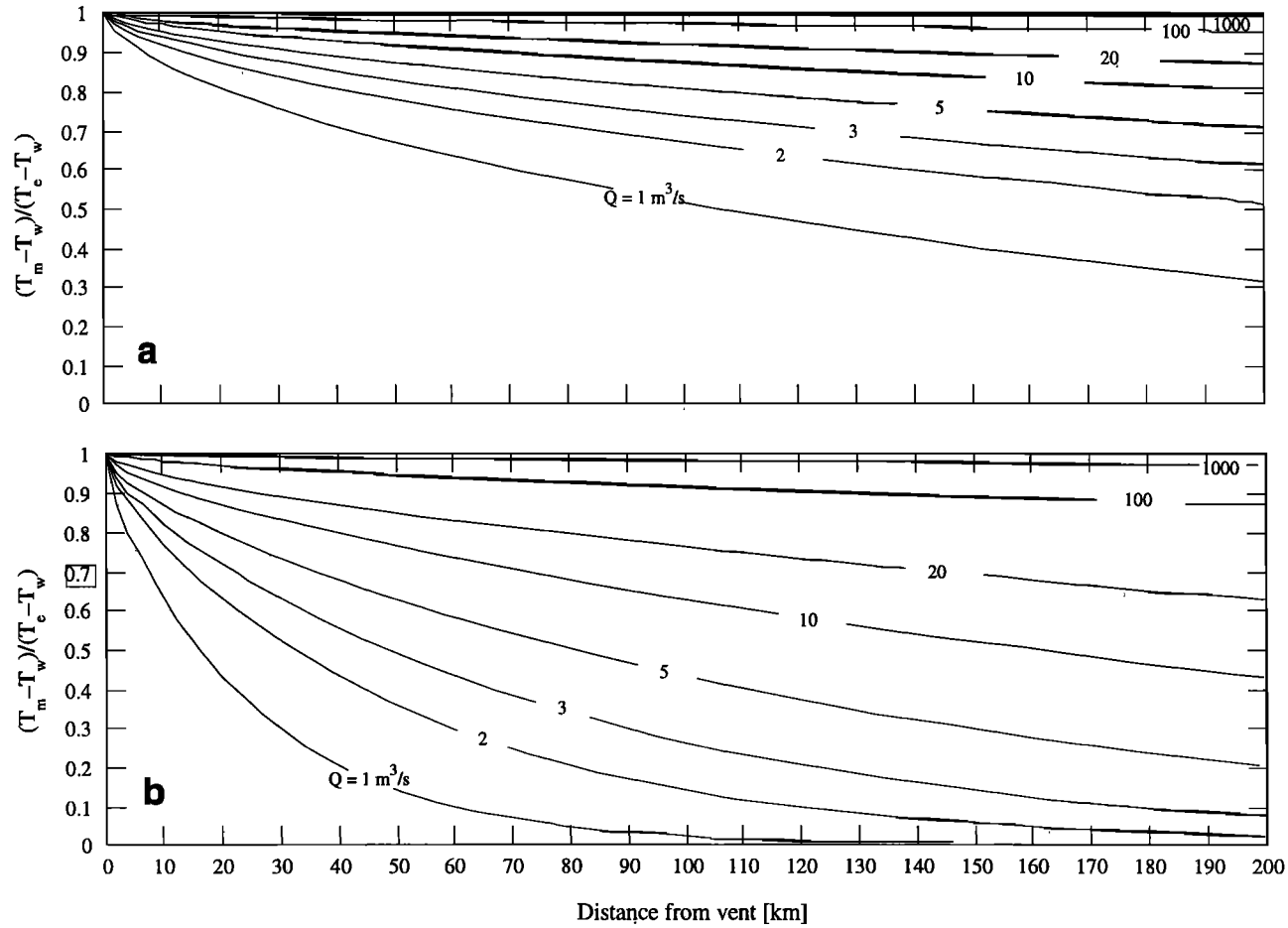

Figure 5. Comparison of the constant temperature wall convective cooling models for the dimensionless mean bulk temperature for up to 200-km-long tubes with flow rates of 1 to 1000 m^3/s. Both plots are for a summation of 500 terms evaluated every 2 km. (a) Circular tube model. (b) Parallel plate model for w=12(2d). Note that for tubes, the temperature solutions are most accurate near T_m=T_w, and become increasingly unrealistic as $T_m \rightarrow T_w$, since the temperature dependence of the viscosity will become important for more than minimal cooling amounts.

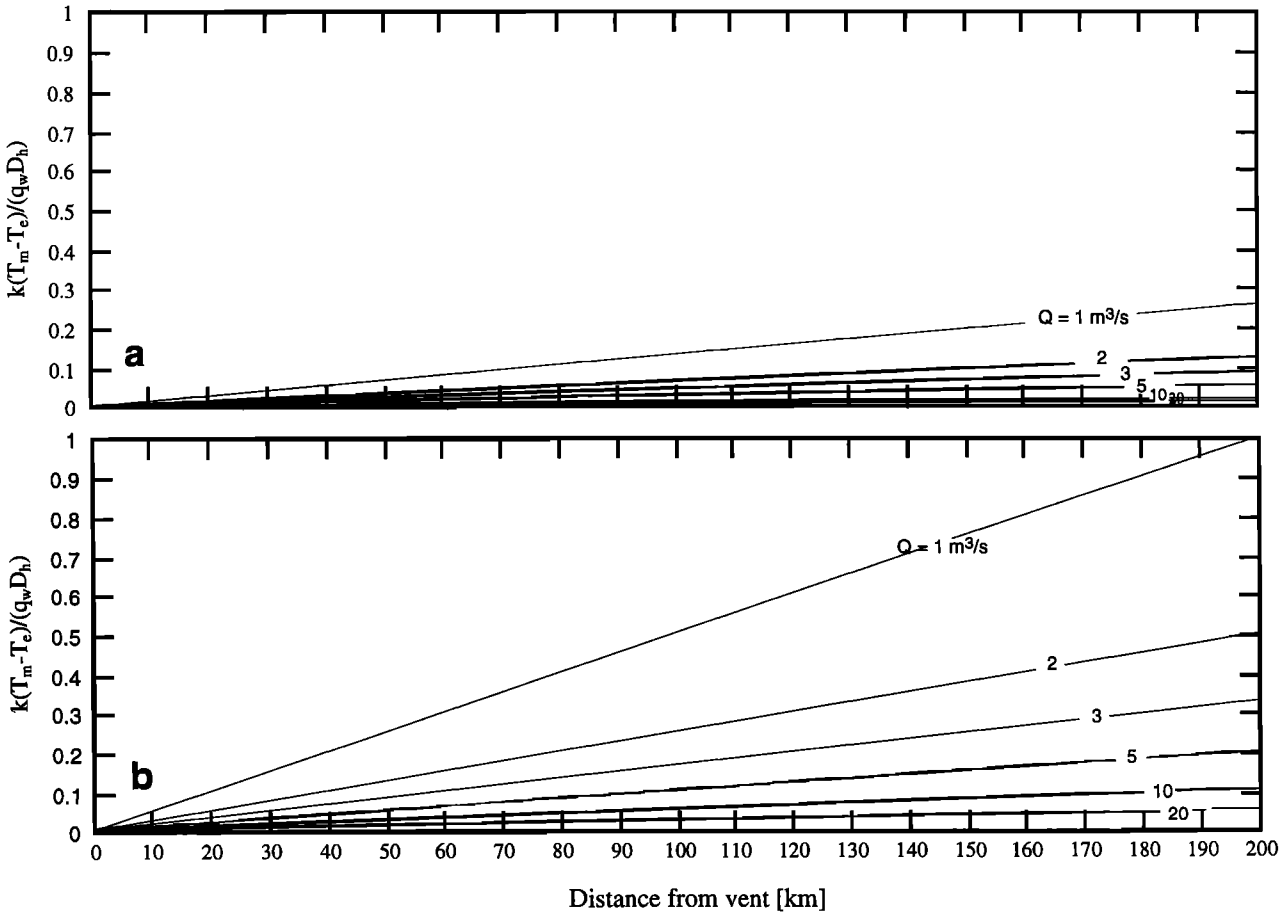

Figure 6. Comparison of the constant wall heat flux convective cooling models for dimensionless mean bulk temperature for up to 200-km-long tubes with flow rates of 1 to 1000 m^3/s. (a) Circular tube model. (b) Parallel plate model for $w=3d$.

distance. Note that the lava tube temperature solutions are most accurate near $T_m=T_w$ and become increasingly unrealistic as $T_m \rightarrow T_w$, since the temperature dependence of the viscosity will become important for more than minimal cooling amounts.

Figure 6 also shows the dimensionless fluid mean bulk temperature versus distance but for the constant wall heat flux solutions for circular tube (equations (3a) and (3c)) and parallel plate (equations (4a) and (4c)) flows. As before, the flow widths for the parallel plate solutions are equal to 12 times the plate spacing. As for the constant temperature solutions, the round tubes are more thermally efficient.

For both types of thermal boundary conditions, the mean temperature versus distance predictions for specific tube flows are found by assuming entrance temperatures, wall temperatures or heat fluxes, and flow rate ranges. The entrance temperatures are normally assumed to be the eruption temperatures, and the flow rates are either observed or a range is found using the driving-force approach described earlier.

3. Predicted Cooling in Long Basaltic Flows

3.1. Waha'ula and Kamoamoa Lava Tubes, Kilauea, Hawaii

The Pu'u 'O'o –Kupaianaha eruption of Kilauea (1983-present) has resulted in the formation of numerous lava tubes [e.g., see *Wolfe et al.*, 1987; *Heliker and Wright*, 1991; *Realmuto et al.*, 1992; *Mattox et al.*, 1993; *Hon et al.*, 1994; *Mangan et al.*, 1995; *Kauahikaua et al.*, 1996]. We have selected data from two of these tubes (the Waha'ula tube and the Kamoamoa tube) for cooling model input.

The Waha'ula tube was part of episode 48 which erupted nearly continuously from the Kupaianaha vent from July 1986 through February 1992 [*Mattox et al.*, 1993; *Hon et al.*, 1994; *Kauahikaua et al.*, 1996]. From April 1991 through February, 1992, the Waha'ula tube carried all of the lava produced at the Kupaianaha vent 12 km to the ocean [*Kauahikaua et al.*, 1996]. *Kauahikaua et al.'s* [1996] measurements of the volumetric flow rate through the tube ranged from 250,000 m^3/d through an approximately linear decrease down to 54,000 m^3/d (2.9–0.625 m^3/s, average value of 1.74 m^3/s). Eruption temperatures for the Kupaianaha vent lava pond for this episode were reported by *Helz et al.* [1991] as 1158°–1161°C, with a maximum of 8°–9°C cooling from the pond to the coast. *Cashman et al.* [1994] sampled the tube at half a dozen skylight, breakout, and coastal spatter locations and reported glass geothermometry temperatures of the samples as ranging from 1153°C at 1.5 km from the vent to 1150°C at the coast, with two breakouts (and thus possibly slightly cooler samples) as the lowest temperature of 1147° (see Figure 1). (See *Helz and Thornber* [1987] and *Helz et al.* [1995] for a discussion of the geothermometry techniques.) Since the lava tube system extended from the Kupaianaha lava pond to the coast [*Heliker and Wright*, 1991; *Realmuto et al.*, 1992; *Mattox et al.*, 1993;

Hon et al., 1994; *Kauahikaua et al.*, 1996], we have assumed the pond temperature to be the tube entry temperature. For the model of this tube, we have assumed tube entrance temperatures of 1158°–1161°C and flow rates of 0.6–3 m^3/s. The transition point between a partially full tube and a full tube is poorly constrained. To find the slopes along the Waha'ula tube and the Kamoamoa tubes, we displayed the preeruption topography contours from the Kilauea volcanology CD-ROM version of the Hawaii Volcanoes National Park map [*Glaze et al.*, 1992; *U.S. Geological Survey*, 1986] over *Cashman et al.'s* [1994, Figure 1] reported tube locations for the temperature measurements and plotted the topographic profiles and slopes along the tube traces in Figure 7. This is more detailed slope data than used in *Keszthelyi's* [1995] thermal model, and it shows a gradually increasing slope from the vent to the Pali until the shallow slopes of the coastal plain are encountered. These data are consistent with estimated slopes of less than 2° near the vent [e.g., *Wolfe et al.*, 1987; J. Kauahikaua, personal communication, 1995], increasing to more than 10° over the Pali, and coastal plain slopes under 2° again. There are no reported skylights for this tube on the coastal plain, and both the Waha'ula tube and the Kamoamoa tubes were feeding inflating flows and so were very likely to be pressurized and full. The slope distribution shown in the Figure 7 could easily produce tubes that have a long transition from partially full to full [*Crisp et al.*, 1995].

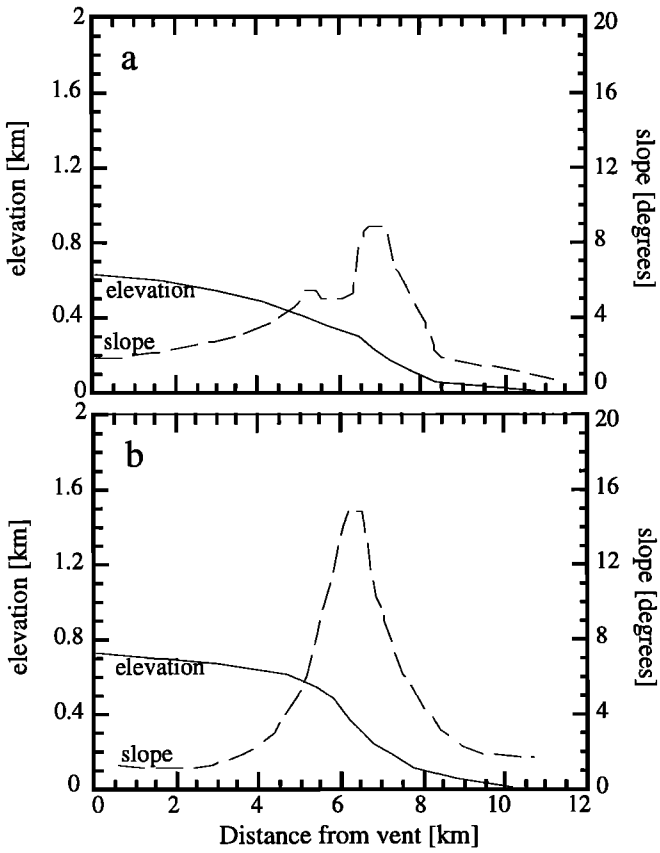

Figure 7. Topographic profiles and slopes along the (a) Kamoamoa and (b) Waha'ula lava tube locations reported by *Cashman et al.* [1994]. For both plots, elevation is plotted along the left y axis and slope along the right y axis. Solid line is the elevation versus distance, and the dashed line is slope versus distance. Vertical exaggeration is approximately a factor of 4.

We examine parallel plate and tube models separately, but given observations of differences in the nature of the flow, as well as the resultant model fits for separate solutions, we are driven to consider combined solutions. Since the depth of the flow in the tube near the vent, where the tubes tend to run partially full, was measured as 0.5–1 m [*Cashman et al.*, 1994; *Kauahikaua*, 1996], we have constructed a piecewise model in which flow near the vent uses the parallel plate model. Farther from the vent where slopes are shallower and tubes tend to run full [*Cashman et al.*, 1993; *Hon et al.*, 1994; *Cashman et al.*, 1994, *Kauahikaua*, 1996] we utilize the circular tube model.

The Kamoamoa tube was part of eruption episode 53 from the Pu'u O'o vent. *Cashman et al.*'s [1994] geothermometry data for the tube samples show temperature results similar to those of the Waha'ula tube, with the highest temperatures of 1154° found 1.1 km from the vent, with values decreasing to 1148°C at the coast (Figure 1). Published data for this episode are not as abundant as for earlier episodes. However, the Pu'u O'o vent regularly erupts lavas about 6°C hotter than those at the Kupaianaha vent [*Heliker and Wright*, 1991; *Helz et al.*, 1991]. Considering this and that the start of the tube was near or at the vent, we have assumed a probable range of tube entrance temperature of 1162°C to 1168°, which were the most recent previous temperatures at this vent [*Helz et al.*, 1991]. C. Thornber's (personal communication, 1997) data from the last several years indicate typical lava tube cooling rates of 0.7°C/km with ranges from 0.5° to 1°C/km depending on flow rate, tube diameter, etc. Eruption rates for this tube are also uncertain, and we have used a range of 0.1–6 m^3/s that is consistent with the range of flow rates observed for other tubes in this eruption [*Heliker and Wright*, 1991; *Kauahikaua et al.*, 1992; *Hon et al.*, 1994; *Zebker et al.*, 1996; *Kauahikaua*, 1996; *Kauahikaua et al.*, 1996]. Slope ranges for the Kamoamoa tube are similar to those of the nearby Waha'ula tube described above.

Figure 8 shows the best cooling model fits for the Waha'ula and Kamoamoa lava tubes with the temperature data of *Cashman et al.* [1994]. Figure 8a compares constant wall temperature circular tube and parallel plate models for a constant temperature boundary of 1077°C, a 1.7 m^3/s flow rate, and some variation in the eruption temperatures. Note that neither the tube or parallel plate model can be fit to the tube along its length. This is expected due to the difference in flow regime between the near-vent and distal parts of the flow. To explain the observed temperature requires a combination of models. The best fit of the constant wall temperature models is shown in Figure 8a; this model has a 12-m-wide by 1-m-deep flow with a gradual change in geometry to a full round tube, a 1.7 m^3/s flow rate throughout its length, and a transition to a full tube after several kilometers where the slopes increase beyond 2°. Figure 8b shows several results for the constant heat flux boundary condition and compares a parallel plate model with a flow depth of 1 m and a width of 12 m to a circular tube model as well as a dual geometry model for a constant wall heat flux of 2 kW/m^2 (within the range shown by *Keszthelyi* [1995]). The best constant flux model fit from within the range of parameters considered (see Table 3) has a flow rate of 1.7 m^3/s, and an initial temperature of 1158° C in a partially full tube for the first few kilometers, with a slow transition to a full round tube using the solution matching method described in the assumptions. Figure 8c shows the Kamoamoa convective cooling models and compares one parallel plate model that is 12 m wide and 1 m deep with a flow rate of 4.5 m^3/s and an

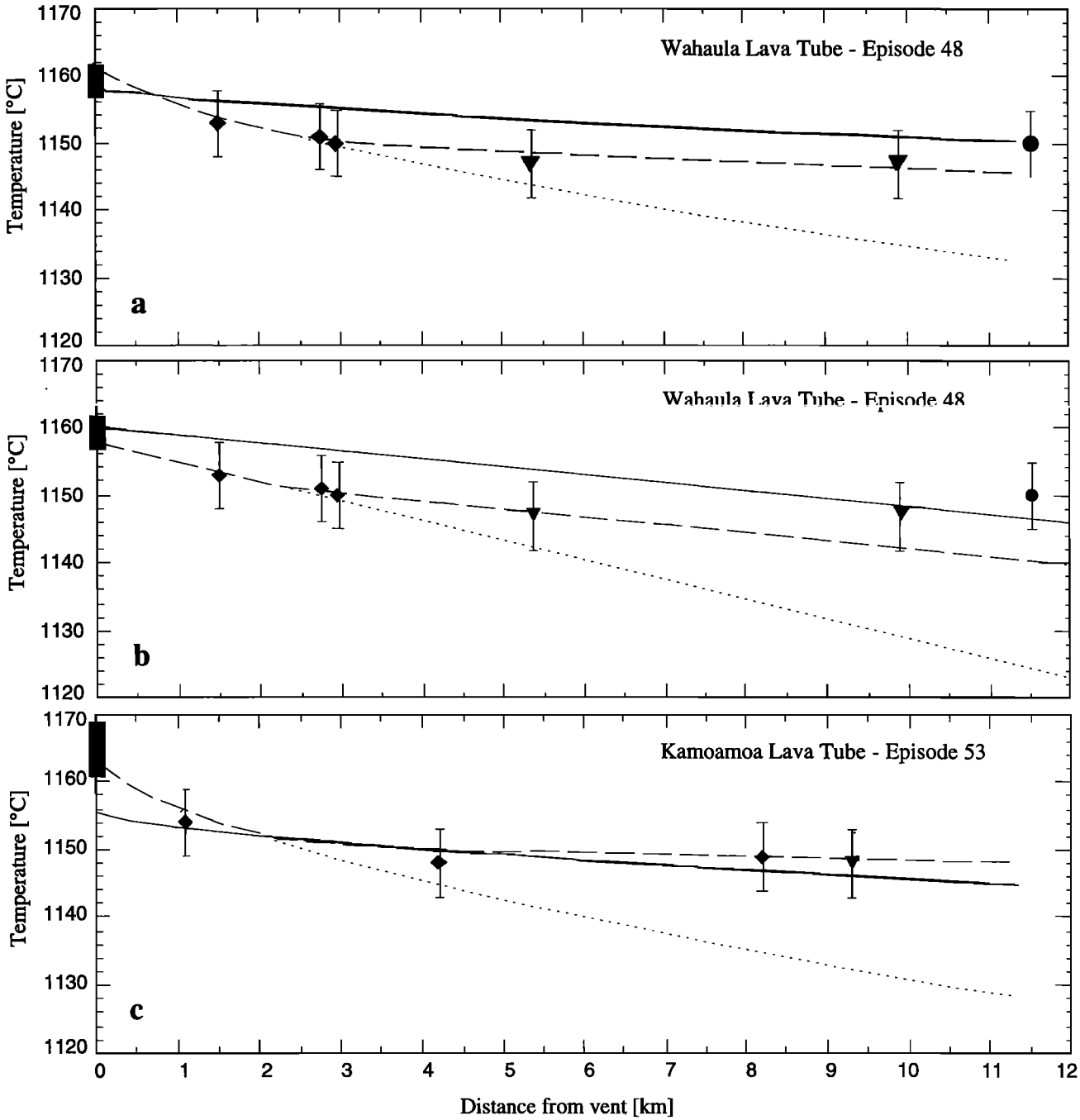

Figure 8. Comparison of convective cooling models for the Waha'ula and Kamoamoa lava tubes plotted with the data from Figure 1. (a) Constant temperature wall models for the Waha'ula tube. The solid line is the temperature predicted for a circular tube with a flow rate of 1.7 m^3/s, a wall temperature of 1077°C, and an initial temperature of 1158°C; the dotted line is the parallel plate cooling model for the same flow rate and an eruption temperature of 1162°C; and the dashed line is a cooling rate predicted by a flow rate of 1.7 m^3/s and an initial temperature of 1162°C in a partially full tube for the first few kilometers, with a slow transition to a full round tube. (b) Constant wall heat flux models for the Waha'ula tube. The solid line is the temperature predicted for a circular tube with a flow rate of 1.7 m^3/s, a wall heat flux of 2 kW/m^2, a tube diameter of 3 m, and an initial temperature of 1160°C. The dotted line is the parallel plate cooling model for the same flow rate, a flow width of 12 m, depth of 1 m, and an eruption temperature of 1158°C, and the dashed line is the cooling predicted by a flow rate of 1.7 m^3/s and an initial temperature of 1158°C in a partially full tube for the first few kilometers, with a slow transition to a full round tube. (c) Constant temperature wall models for the Kamoamoa tube. The solid line is the temperature predicted for a circular tube with a flow rate of 4.5 m^3/s, wall temperature of 1077°C, and initial temperature of 1156°C. The dotted line is the parallel plate cooling model for a flow rate of 4.5 m^3/s and an eruption temperature of 1164°C, and the dashed line is the cooling predicted by a flow rate of 4.5 m^3/s and an initial temperature of 1164°C in a partially full tube for the first several kilometers, with a slow transition to a full round tube.

eruption temperature of 1164°C with a circular tube model with a wall temperature of 1077°C, an initial temperature of 1156°C, and a flow rate of 1 m^3/s. The 12:1 aspect ratio here is primarily for comparison to the Waha'ula tube, since the published data on the Kamoamoa tube have little tube size information. The best fit is with a dual geometry model with an 1164°C eruption temperature and a partially full (12 m wide and 1 m deep) tube that makes a gradual transition after several kilometers to a circular tube with the same flow rate and wall temperature. The constant heat flux models for Kamoamoa provide similar results to those shown with the Waha'ula tube, and here it also tends to overpredict the cooling near the end of the tube and to underpredict it near the front, even when fit with a dual geometry model. Section 4 illustrates some of the effects of systematic variations in the flow rate, entrance temperature, and wall temperature for the parallel plate and circular tube models. Higher cooling rates for the constant flux circular tube flow models can be obtained by decreasing their depth of burial, but they will still consistently underpredict the cooling on the upper slopes.

For both tubes, the thermal losses in the distal regions of the flow are well fit by the full circular tube models, but the heat losses in the vicinity of the vent are still an open question. The dual geometry models presented here are one possible explanation for the apparently higher near-vent thermal losses, but we recognize that other mechanisms and model parameter adjustments may fit the data equally well. However, without additional data, we cannot distinguish between the appropriateness of this dual geometry model and a variety of more complex model approaches.

3.2. Flows From the Undara, Toomba, and Kinrara Volcanoes, Queensland, Australia

The Undara, Toomba, and Kinrara volcanoes are sources for three of the long basaltic lava flows found in North Queensland that may have been tube-fed [*Atkinson et al.*, 1975; *Stephenson and Griffin*, 1976; *Stephenson et al.*, 1980; *Atkinson and Atkinson*, 1995]. All three of these flows are on shallow slopes and show little petrographic or textural variation from vent to end, which suggests minimal cooling and tube flow rather than surface flow. They all have either drained tubes and collapse pits or inflation features common to tube-fed basaltic flows on low slopes [e.g., *Stephenson et al.*, 1996; *Whitehead and Stephenson*, this issue] similar to those seen in Hawaiian flows [e.g., *Cashman et al.*, 1993; *Hon et al.*, 1994; *Kauahikaua et al.*, 1996; *Kauahikaua*, 1996]. The ranges used for eruption temperature, flow length, and flow rates are shown in Table 3. The flow rate range encompasses some very large flow rates as well as the low rates favored by *Stephenson et al.* [1996] to include the possibility that the largest tubes might have flowed full (particularly in the early stages of the eruption), although field evidence of numerous flow levels at Undara suggests that the largest tubes flowed partially full at least some of the time [*Atkinson and Atkinson*, 1995].

The 190,000-year-old Undara volcano in the McBride volcanic province of Queensland, Australia, is well known for its lava tubes and has generated some very long lava flows, including one that is more than 160 km long on an average slope of 0.3°, with numerous lava tube collapse pits, caves, inflation features, and depressions [*Stephenson et al.*, 1980]. Other features in the flow include possible "conduit systems" which may be tube networks rather than a single tube, since they are on the lowest slopes along the flow of <0.1°, and show evidence for flow inflation, which is commonly a tube-fed phenomenon [*Hon et al.*, 1994]. There is also evidence for thermal or thermomechanical erosion by the lava tubes [*Stephenson*, 1996 p. 82]. Undara has similar petrography from end to end, and P.J. Stephenson (personal communication, 1997) found composition melt temperatures at the distal end of 1150°. The region proximal to the vent of the same unit has been buried by subsequent flows, but the petrographic variation from end to end is similar to that at Toomba, and so here we have assumed that the temperature variations were similar also. Some of the Undara lava tube caves show evidence of flow levels [*Atkinson and Atkinson*, 1995] and so may have been similar in places to the partially full tubes on the upper slopes of Kilauea's Pu'u O'o-Kupaianaha eruption [e.g., *Hon et al.*, 1994; *Kauahikaua et al.*, 1996]. However, without detailed temperature data, there are few constraints on which of several cooling models might be most accurate.

The 13,000 year old Toomba basalt flow in the Nulla volcanic province of Queensland, Australia is 123 km long on an average slope of 0.2° [*Stephenson and Griffin*, 1976; *Stephenson et al.*, 1996; *Whitehead and Stephenson*, 1996] and has well-preserved pahoehoe inflation structures that are presumed to be tube-fed, although the tubes are assumed to have solidified under the flow undrained [*Stephenson and Whitehead*, 1996]. Although the Toomba flow followed the bed of the Burdekin river, the absence of pillow basalt and hyaloclastite features at the flow base has led to the interpretation that the

Table 3. Assumed Tube Flow Parameters

Tube	Length, km	Eruption Temperature Range, °C	Flow Rate Range, m^3/s
Waha'ula Tube (Kilauea, Hawaii)	11.5	1158–1162	0.6–3 (1.7)
Kamoamoa Tube (Kilauea, Hawaii)	12	1162–1168	0.1–6
Undara Flow (Queensland, Australia)	160	1155–1165	1–1000
Toomba Flow (Queensland, Australia)	123	1150	1–1000
Kinrara (Queensland, Australia)	50	1160	1–1000
Alba Patera, Mars	200	1145–1170	1–100,000

river was at dry season levels and may not have been flowing on the surface during flow emplacement [*Stephenson,* 1996]. The flow may have encountered isolated water holes [*Stephenson and Whitehead,* 1996], and there is evidence of interaction of water with the solid but still hot flow [*Stephenson,* 1996]. The general absence of lava channels and aa lava and an abundance of inflation features led *Stephenson et al.* [1996] to favor low effusion rates (5–10 m^3/s). Petrologic relationships combined with some melt modeling and a series of glass analyses indicate an eruption temperature of 1150°C, with possibly 10° of apparent cooling, although glass alteration has obscured some of the relationships and made the interpretation of the results problematic (P.J. Stephenson, personal communication, 1997).

The 20,000-year-old Kinrara volcano in the McBride volcanic province of Queensland, Australia, generated basanite lavas that flowed 65 km over an average slope of 0.4° [*Stephenson et al.,* 1980, 1996]. The effusion rate for this volcano was probably higher (or less steady) than for Undara and Toomba, since the crater formed a spatter rim, and aa lavas make up a relatively larger percentage of the flows [*Stephenson et al.,* 1996]. However, a number of flow inflation features and drained lava tubes indicate that the flows were tube-fed to at least some extent. From melt modeling and comparisons to the Toomba and Undara compositions, the eruption temperature may have been somewhat higher (perhaps 1160°C (P.J. Stephenson, personal communication, 1997)).

Figure 9 shows the results for the Undara model which is a constant wall temperature model for an eruption temperature of 1160°C and wall temperatures of either 1077° or 1130°. Results are shown for flow rates of 1 to 1000 m^3/s. The lower wall temperature model is more appropriate for a more established tube, where the wall location has reached equilibrium at the isotherm of the effective solid. The hotter wall temperature may be more appropriate for regions of the flow where the tube was less distinct, either as part of a network of closely spaced flow paths or as part of an internal region of concentrated flow. For the lower wall temperatures, the circular tube model requires flow rates of approximately 10 m^3/s or more to avoid temperature drops that would produce substantial rheology changes, and the parallel plate model would require flow rates of approximately 40 m^3/s or more. The higher wall temperatures would allow lower rates of 2 and 20 m^3/s for the circular tube and parallel plate models, respectively. The models for the Toomba flow used a lower eruption temperature of 1150°C but had a slightly shorter flow length and resulted in nearly identical cooling predictions and flow rate restrictions. The Kinrara models used the same parameters as the Undara models, and the results for the Kinrara flow can be read from Figure 9 at the 50–km Kinrara tube length. The shorter (50 km) flow length allows most of the lowest flow rates of 1–5 m^3/s to reach the end of the flow with less than 10° cooling for the hotter wall temperature of 1130°, and flow rates of 10–50 m^3/s are required for the cooler wall temperatures. As for Undara, the lower wall temperature model is more appropriate for the more established tube and the hotter wall temperature for the less established tube or tube-like internal flow networks.

3.3. Alba Patera Lava Tubes, Mars

Alba Patera is an extensive volcanic structure on the northern portion of the Tharsis region of Mars. With a summit that is about 7 km above the surrounding terrain and a diameter of 1600 km, the average slopes are thought to be <0.5° [*Carr,* 1981; *Cattermole,* 1990]. Alba has numerous lava flows up to hundreds of kilometers long with a ridged cross section, many with chains of depressions thought to be collapse pits [*Carr et al.,* 1977; *Cattermole,* 1987, 1990; *Mouginis-Mark et al.,* 1988; *Schneeberger and Pieri,* 1991; *Hodges and Moore,* 1992]. Previous work [*Sakimoto et al.,* 1997] on the relationships between tube dimensions, driving forces, and effusion rates and rheology parameters was applied to Alba Patera and suggests effusion rates somewhere between 2 and 10^5 m^3/s and viscosities between 10^2 and 10^6 Pa s. *Sakimoto et al.* [1997] also estimated common tube diameters from the minimum collapse depression sizes at 50-100 m and typical flow lengths of 50-100 km from the lengths of the collapse depressions chains. For this study, we have modeled a representative flow that is 200 km long, with effusion rates from 1 to 10^5 m^3/s (Table 3). For the parallel plate model, the flow width was assumed to be 100 m, and we arbitrarily set the flow depth to 20 m. We have used a range of eruption temperatures of 1145° to 1170°C on the assumption that the flows were probably basaltic [e.g., *Carr et al.,* 1977], though this parameter is obviously poorly constrained.

Figure 10 shows the model results for the constant temperature wall convective cooling models for the Alba Patera lava tubes. For this set of predictions, the circular tube flow rates would need to be at least 10 m^3/s to avoid significant viscosity increases before a 200–km flow length was reached and greater than about 2 m^3/s for the 50–km tube. For the parallel plate flow, the thermal losses are larger, and the flow rates would need to be ~40 m^3/s through the 200–km tube and nearly 20 m^3/s or greater for the 50–km–long tube.

4. Discussion

Constant wall temperature convective cooling models predict a nonlinear cooling rate as a function of distance for lava tubes. However, for those flows for which we have the most detailed temperature measurements, there are variations in the geometry of the tube flow regime, and no single model can adequately fit the data within published uncertainties. A constant wall temperature model that combines a tube solution at the distal part of the tube (where slopes are shallow and tubes run full) with a parallel plate model in the near-vent region (that takes into account radiative loss where slopes are higher and tubes run partially full), can explain the Waha'ula and Kamoamoa lava tube temperature measurements. The constant heat flux solutions yield a constant cooling rate with distance that is not as good a fit to the data where we have detailed information on the tube temperature versus distance. As in *Keszthelyi's* [1995] model, the constant heat flux model will yield a different cooling rate if it is evaluated for each different tube section diameter, but the rates are still piecewise linear, and the additional diameter information is necessary to predict the mean tube temperature variation with distance. This constant heat flux assumption also implies that the wall temperature cannot be constant along the length of the flow. Likewise, the higher heat flux rates near the tube entrance required by the constant temperature wall models seem consistent with *Realmuto et al.'s* [1992] data, as well as theoretically reasonable, since the temperature differences between the initial lava temperature and the ambient conditions are likely to be larger.

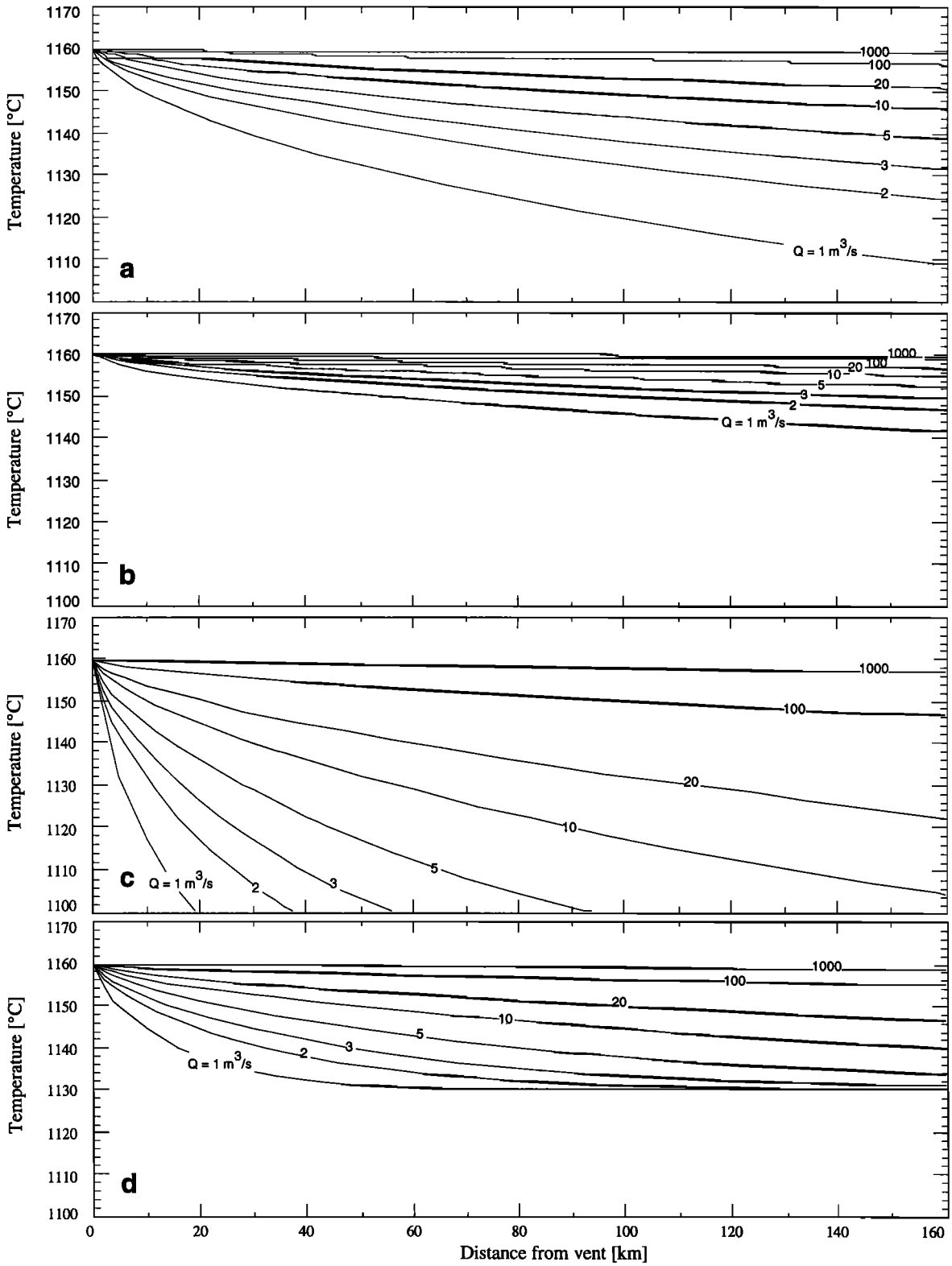

Figure 9. Comparison of constant temperature wall convective cooling models for the Undara lava tube with contours for flow rates of 1, 2, 3, 5, 10, 20, 100, and 1000 m^3/s. (a) Temperatures predicted for a circular tube with an entrance temperature of 1160°C and wall temperature of 1077°C. (b) Temperatures predicted for a circular tube with an entrance temperature of 1160°C and a wall temperature of 1130°C. (c) Temperatures predicted for parallel plate flow with a height of 1 m and a width of 5 m with an entrance temperature of 1160°C and wall temperature of 1077°C. (d) Temperatures predicted for parallel plate flow with a height to width ratio of 1:5, an entrance temperature of 1160°C and wall temperature of 1130°C. As in Figure 5, the temperature solutions are most accurate near $T_m=T_w$, and become increasingly unrealistic as $T_m \rightarrow T_w$, since the temperature dependence of the viscosity will become important for more than minimal cooling amounts.

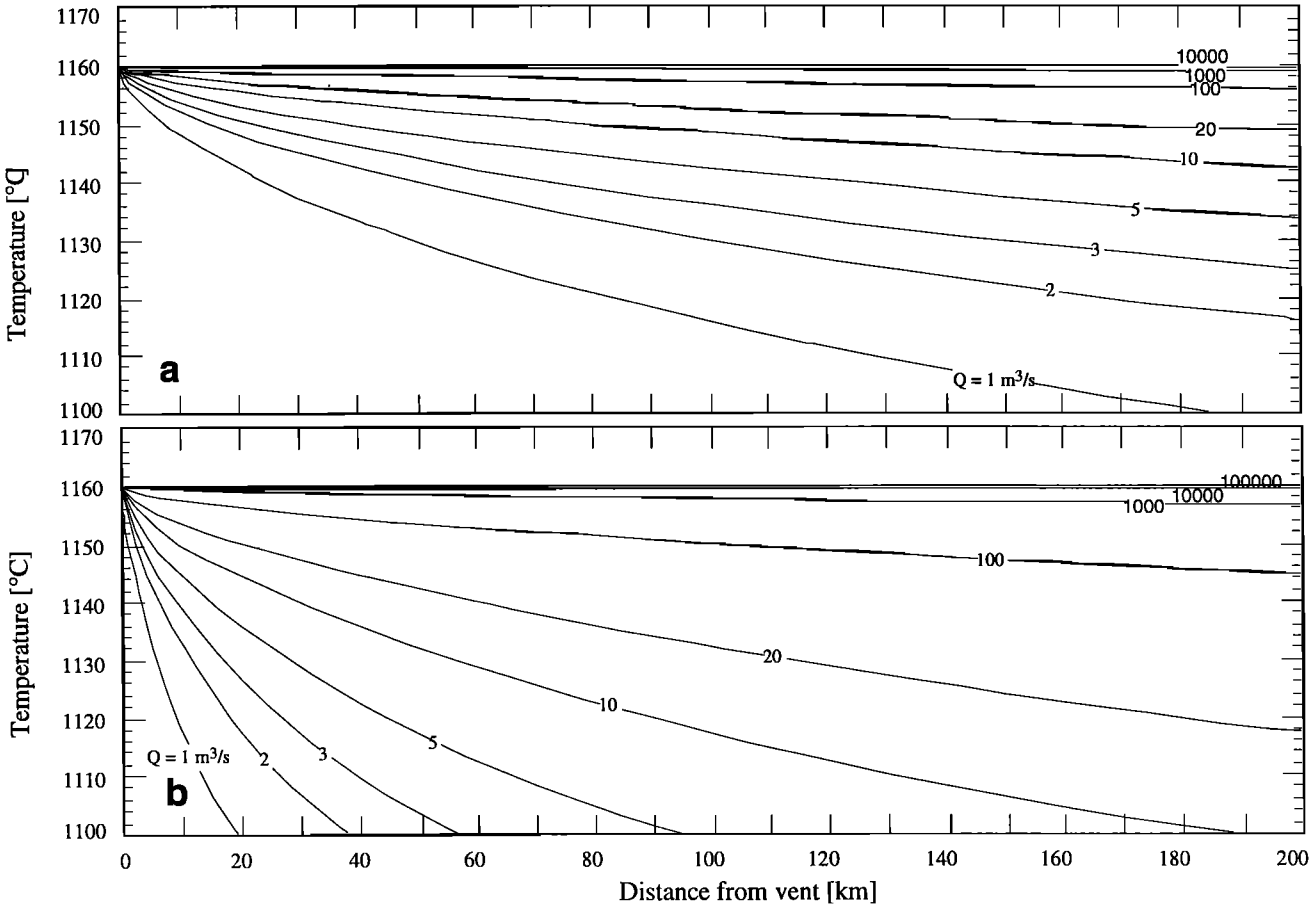

Figure 10. Comparison of constant temperature wall convective cooling models for the Alba Patera lava tube with contours for flow rates of 1 to 10^5 m^3/s. (a) Mean bulk temperatures predicted for a circular tube with an entrance temperature of 1160°C and wall temperature of 1077°C. (b) Temperatures predicted for parallel plate flow with a height:width ratio of 1:5, an entrance temperature of 1160°C, and a wall temperature of 1077°C.

Within the cooling predictions of the constant wall temperature models, the use of an accurate flow rate yields more reliable cooling rate results than modeling cooling rates with flow rates from slopes or driving pressures. With a flow rate approach and the constant wall temperature models, the aspect ratio of the flow affects the cooling more than the flow rate. With this in mind, a parallel plate flow approximation with an accurate flow rate is arguably a better cooling model approximation for partially full tubes in Hawaii than the circular tube model and yields a very good fit to the available data for the upper 3 km of the partially full Waha'ula tube. Additionally, wall temperatures in the range of 1070°–1130°C work well in these models. They are consistent with prior estimates of either where the basalt makes a transition to a rheological solid (55% crystals [*Marsh*, 1981]) or where, in the margins of small or slow flow systems, the crystal content and shear strength are not yet close to the 55% crystallinity but are large enough to retard flow and act as a wall (e.g., 15–55% crystals in small tubes [*Sakimoto*, 1995b, also unpublished data, 1997]).

The above results for the tubes were selected to show some of the best fits of the models to the data. In order to show some of the variations expected in the predicted temperatures as a function of input parameter variations, Figures 11 and 12 show the circular tube and parallel plate constant wall temperature models for systematic variations in flow rate, entrance temperature, wall temperature, and flow width (for the parallel plate model). For both geometries, the steepest cooling rates are at the entrance, and wall temperatures of 1077° provide reasonable data fits, although a combination of higher wall temperatures and a shallower tube will yield similar results. For Figure 12, the range of flow widths shown extends from w/D = 8 to 40. The lower end of the range will tend to underpredict cooling, since the effects of heat loss from the sides of the flow will be a significant fraction of the total heat losses.

If additional information is available for a particular tube on burial depth variations or other factors that might introduce a significant axial variation in the temperature or heat flux boundary condition, there are a few analytic solutions available that factor in axial variations in wall heat flux or temperature [*Shah and London*, 1978]. For example, for a linear variation in wall temperature for the circular tube, see *Sellars et al.* [1956], or for wall heat flux variations, see *Bhattacharyya and Roy* [1970]. Predictably, wall temperatures are higher where heat flux rates are higher. One main effect of such axial variations is the lengthening of the thermal entrance length.

Figure 13 compares the thermal losses from a strictly conductive (static lava) cooling solution to those calculated from the convective circular tube constant wall temperature solution presented here. It is a plot of the ratio of the heat flux per unit area versus distance from the tube entrance for the

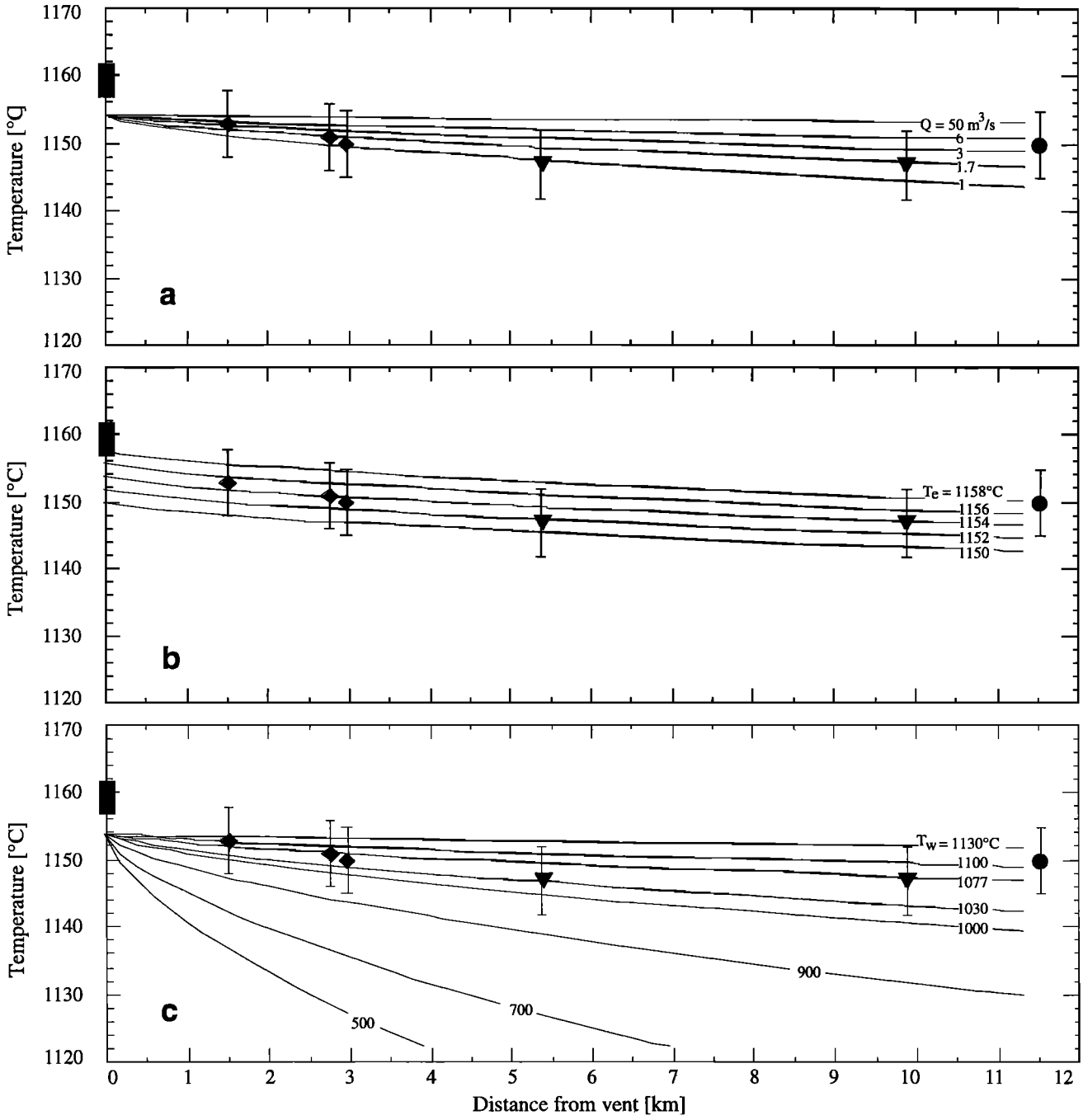

Figure 11. Comparison of constant wall temperature circular tube convective cooling models for systematic variations in flow rate, entrance temperature, and wall temperature. (a) The constant wall temperature circular tube model with an entrance temperature of 1154°C, wall temperatures of 1077°C, and flow rates of 1-50 m^3/s. (b) The same model for flow rates of 1.7 m^3/s ,wall temperatures of 1077°C, and entrance temperatures of 1150°C to 1158°C. (c) The same model for flow rates of 1.7 m^3/s and entrance temperatures of 1154°C and wall temperatures from 500° to 1130°C.

circular tube model and the heat flux per unit area for the conductive cooling solution used in Figure 3 and by *Keszthelyi* [1995]. The heat flux per unit area for the convective model is calculated from the definition of the local Nusselt number, $Nu_{z,T} = [q_w(z)\, D_h]/(T_w - \theta_m)$ [*Shah and London*, 1978], where θ_m is given by equation (A7) and $Nu_{z,T}$ is given by equation (A17). While the heat flux per unit area in the convective solution may start at larger flux rates than those predicted from the conductive solution, the flux rates decrease rapidly as the thermal boundary layer grows. The conductive solution of Figure 3 assumes a constant temperature (solid) source to calculate the heat flux, and does not treat either the thermal boundary layer or the heat carried down the tube by the fluid. For shorter tubes such as the 10 km tubes in Hawaii, the total thermal losses for both solutions may be similar, but for longer tubes, the thermal losses from the convective solutions will be far less than those in the conductive solutions.

For partially full tubes, the assumption of a flow surface cooler than the flow interior allows the formation of a temperature gradient within the flow near the surface that is

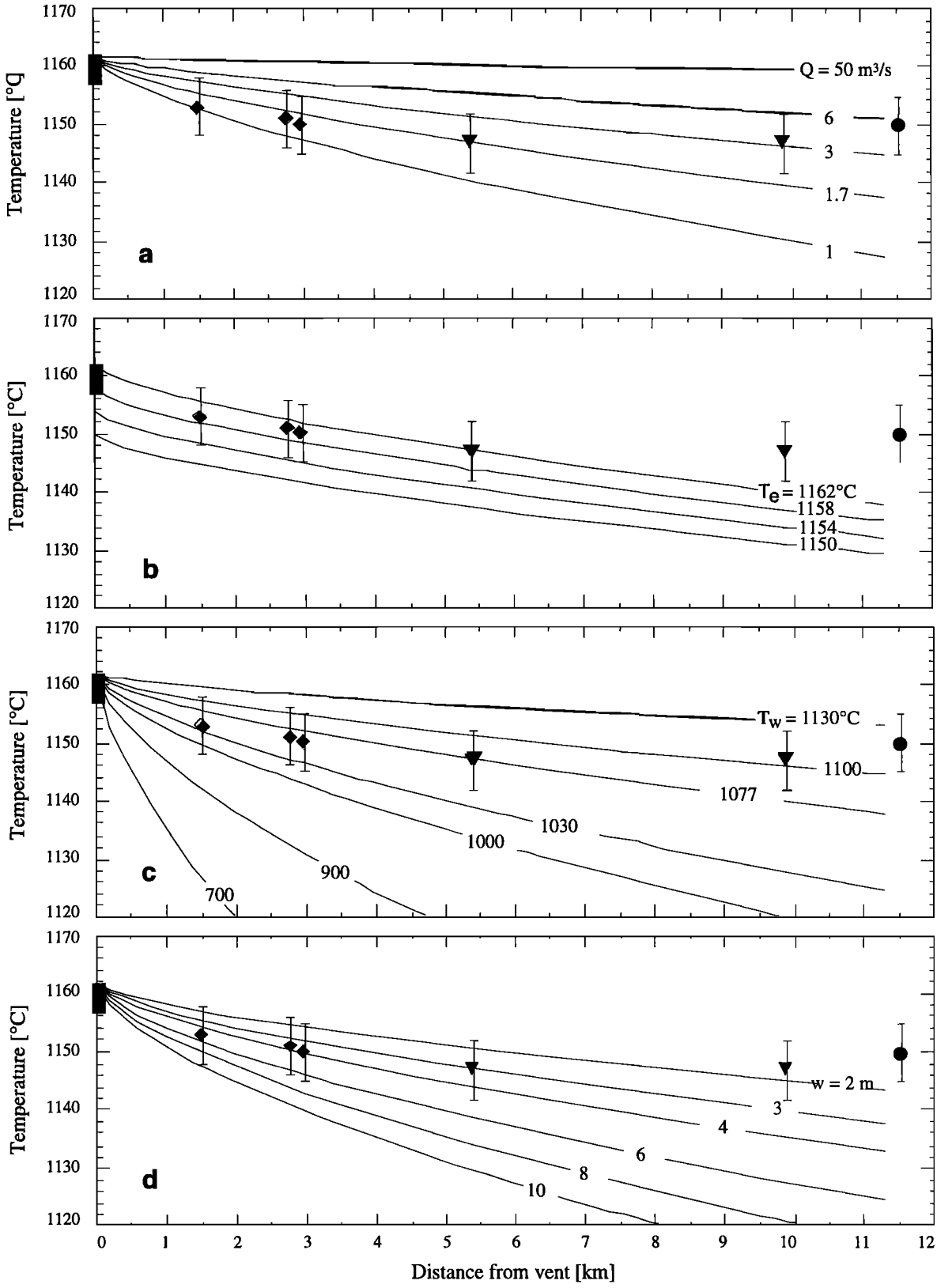

Figure 12. Comparison of constant wall temperature parallel plate convective cooling models for systematic variations in flow rate, entrance temperature, wall temperature, and aspect ratio. (a) The constant wall temperature parallel plate model with an entrance temperature of 1162°C, flow depth of 1 m, flow width of 12 m, and flow rates of 1-50 m^3/s. (b) The same model for flow rates of 1.7 m^3/s, wall temperature of 1077°C, and entrance temperatures of 1150°C to 1162°C. (c) The same model for flow rates of 1.7 m^3/s and entrance temperatures of 1162°C and wall temperatures from 700°C to 1130°C. (d) The same model for flow rates of 1.7 m^3/s and entrance temperatures of 1162°C, wall temperatures of 1077°C, and flow widths from 8 m to 40 m.

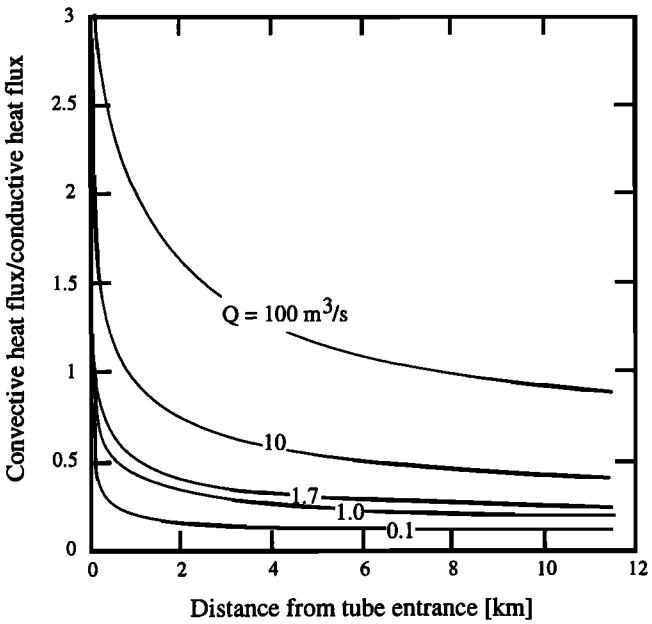

Figure 13. Plot of the ratio of the heat flux per unit area versus distance from the tube entrance for the circular tube constant temperature wall convective cooling model and the heat flux per unit area for the conductive cooling solution used in Figure 3 and by *Keszthelyi* [1995]. The heat flux per unit area for the convective model is calculated from equations (A7) and (A17) and the local Nusselt number (see text). While the heat flux per unit area in the convective solutions may start at larger values than those predicted from the conductive solution, the flux rates decrease rapidly as the thermal boundary layer grows.

similar to those at the sides of the flow. If the difference is at least a few degrees, the heat transfer rates within the flow will again be the limiting cooling processes. However, if the flow surface is not significantly cooled by the radiative transfer, then the effective perimeter of the tube is that of the flow/wall rock boundary plus that of the cavity/wall rock boundary, and either the parallel plate approximation should be used for the entire perimeter or another problem geometry needs to be assumed. Until measurements of tube cavity temperatures are available, it will not be clear what approach is most appropriate. However, if a tube runs less than full, it is clear that neither a convective tube solution nor a conductive solution adequately explains the cooling near the vent.

These convective models have other immediately apparent volcanologic uses, such as using the parallel plate model for considering the cooling during the emplacement of flood basalts [*Ho and Cashman*, 1997] as insulated internal flow. Note that these models should not be applied to turbulent flows, since heat transfer and flow rates in turbulent flow differ significantly from those in laminar flow.

5. Conclusions

For a range of moderate flow rates and tube entrance temperatures, a combination of forced convective cooling models for parallel plate and tube flow with constant wall temperature boundary conditions yields cooling rates near the tube entrance that are consistent with the Waha'ula and Kamoamoa tube temperature measurements, as well as minimal total cooling rates (<10°–15°C) for flow lengths from 10 to 200 km. The same forced convection cooling process may be applicable to explain the existence of similar flow morphologies for long tube-fed basaltic lava flows in a wide variety of locations, since no local variations in cooling conditions are required, and small variations in eruption temperature or flow rate can accommodate the entire range of flow lengths considered. Our analysis thus suggests that long basaltic flows may be a reflection of low slopes and a particularly steady, moderate, eruption rate, and the slow heat transfer may be characteristic of forced convective cooling rather than of a particular composition.

Appendix: Convective Cooling Models for Tube and Parallel Plate Flow

A1. Laminar Forced Convective Circular Tube Flow With Constant Wall Temperature

This solution is known as the Grätz or Grätz-Nusselt problem and was originally solved for slug flow (flat velocity profile) by *Grätz* [1883]. It was re-solved for a parabolic velocity profile (Poiseuille flow) by Nusselt, Grätz, and others and was extended to cover the constant heat flux boundary problem as well as other boundary conditions and flow geometries. See *Shah and London* [1978], *Burmeister* [1993], or *Kakaç and Yener* [1995] for summaries of the problem development for both types of boundary conditions, and *Shah and London* [1978], *Bird et al.* [1987], *Burmeister* [1993], or *Kakaç and Yener* [1995] for comparisons of various cross-section and boundary condition solutions.

For the circular full tube with a constant wall boundary temperature in laminar Newtonian flow, with no viscous dissipation, crystallization, or temperature dependent properties, and no conduction in the z direction, the energy equation is

$$\frac{\partial^2 T}{\partial r^2}+\frac{1}{r}\frac{\partial T}{\partial r}=\frac{\rho C_p}{k}v_z\frac{\partial T}{\partial z} \tag{A1}$$

where v_z is the axial velocity distribution, the terms on the left are heat conduction in the r direction, and the term on the right is heat convection in the z direction [e.g., *Bird et al.*, 1987, equation 4.4-7]. The accompanying initial and boundary conditions are

$$T=T_e=\text{const} \quad z\le 0 \tag{A2}$$

$$T=T_w=\text{const} \quad r=a \tag{A3}$$

$$\frac{\partial T}{\partial r}=0 \quad r=0. \tag{A4}$$

The axial velocity distribution for Newtonian flow is

$$v_z=2V\left(1-\frac{r^2}{a^2}\right) \tag{A5}$$

where the mean velocity $V=Q/A$.

The Grätz solution for the lava temperature as a function of distance down the tube uses separation of variables to obtain an infinite series solution in terms of eigenvalues and eigenfunctions. This approach is most accurate for distances far down the tube or pipe but can be unwieldy very close to the pipe entrance where the number of terms required for an accurate solution is very large. However, computational advances have

made large summations tractable and the Grätz solution reasonable for the entire tube length in lava tube problems. In practice, considering tube temperatures within a few kilometers of the tube entrance requires at least 50 and sometimes several hundred terms, while accurate temperatures near the entrance (e.g., $L < 50D_h$) may easily require more than 500 terms. Solution accuracy is evaluated by increasing the number of terms until the dimensionless mean bulk temperature converges within the z^* range desired.

Since most lava flows or tubes are simply sampled for temperature as a function of either distance from the vent or time, solutions will be presented for the fluid bulk mean temperature T_m, which is sometimes also called the flow average temperature or the mixing cup temperature. It is the temperature that would be obtained if, at the designated axial distance, the cross section of fluid was mixed before sampling.

The Grätz expressions for the dimensionless fluid temperature and the dimensionless fluid bulk mean temperature [e.g., *Burmeister*, 1993; *Shah and London*, 1978] are

$$\theta = \frac{T - T_w}{T_e - T_w} = \sum_{n=0}^{\infty} C_n R_n \exp\left(-2\lambda_n^2 z^*\right), \tag{A6}$$

and

$$\theta_m = \frac{T_m - T_w}{T_e - T_w} = 8\sum_{n=0}^{\infty} \frac{G_n}{\lambda_n^2} \exp\left(-2\lambda_n^2 z^*\right) \tag{A7}$$

respectively, where λ_n, R_n, and C_n are eigenvalues, eigenfunctions, and constants, and z^* is the dimensionless axial distance

$$z^* = \frac{z}{D_h Pe} = \frac{z}{D_h Re Pr} = \frac{zk}{\rho C_p V D^2} \tag{A8}$$

or, if the solution is desired in terms of flow rate,

$$z^* = \frac{\pi}{4}\frac{zk}{\rho C_p Q} \tag{A9}$$

where D_h is the hydraulic diameter (=4area/wetted perimeter [e.g., *White*, 1991]), D is the tube diameter, and Q is the volume flow rate. For volume flow rates from 1 m^3/s to 10^3 m^3/s and tube lengths of less than 1000 km, z^* ranges from 10^{-8} to 10^{-1}. The values of λ_n, and $G_n = -(C_n/2)R_n'(1)$ have been tabulated in numerous sources, and the first 11 values are shown in Table A1 [*Brown*, 1960; *Shah and London*, 1978].

Table A1. Circular Pipe Infinite Series Solution Functions for a Constant Wall Temperature

n	λ_n	G_n
0	2.7043644199	0.748774555
1	6.6790314493	0.543827956
2	10.6733795381	0.462861060
3	14.6710784627	0.415418455
4	18.6698718645	0.382919188
5	22.6691433588	0.358685566
6	26.6686619960	0.339622164
7	30.6683233409	0.324062211
8	34.6680738224	0.311014074
9	38.6678833469	0.299844038
10	42.6677338055	0.290124676

Brown [1960] and *Shah and London* [1978, Table 12].

Values for the higher ($n \geq 11$) eigenvalues and eigenfunctions may be calculated from *Shah and London* [1978, equations (204) through (207)]

$$\lambda_n = \lambda + S_1\lambda^{-4/3} + S_2\lambda^{-8/3} + S_3\lambda^{-10/3} + S_4\lambda^{-11/3} + O\lambda^{-14/3} \tag{A10}$$

where

$$\lambda = 4n + (^8/_3) \quad n = 11, 12, 13 \ldots$$

$$S_1 = 0.159152288$$

$$S_2 = 0.011486354 \tag{A11}$$

$$S_3 = -\ 0.224731440$$

$$S_4 = -\ 0.033772601$$

and R_n' and C_n may be expressed as $G_n = -(C_n/2)R_n'(1)$, and calculated from

$$G_n = \frac{C}{\lambda_n^{1/3}}\left[1 + \frac{B_1}{\lambda^{4/3}} + \frac{B_2}{\lambda^{6/3}} + \frac{B_3}{\lambda^{7/3}} + \frac{B_4}{\lambda^{10/3}} + \frac{B_5}{\lambda^{11/3}} + O\left(\lambda^{-4}\right)\right] \tag{A12}$$

where

$$G_n = -\left(C_n/2\right) R'_n(1)$$

$$\lambda = 4n + (^8/_3) \quad n = 11, 12, 13 \ldots \tag{A13}$$

$$C = 1.012787288$$

and

$$B_1 = 0.144335160$$

$$B_2 = 0.115555556$$

$$B_3 = -\ 0.21220305 \tag{A14}$$

$$B_4 = -\ 0.187130142$$

$$B_5 = 0.0918850832$$

Calculating R_n for evaluating equation (A6) requires slightly more effort, since it is a function of both n and r/a. It may be evaluated with the series

$$R_n = \sum_{i=0}^{\infty} A_{ni}\left(\frac{r}{a}\right)^i \tag{A15}$$

where A_{ni} is a function of the eigenvalues (λ_n)

$$A_{ni} = 0 \quad i < 0$$

$$A_{ni} = 1 \quad i = 0 \tag{A16}$$

$$A_{ni} = -\lambda_n^2\left(A_{i-2} - A_{i-4}\right)/i^2$$

[*Brown*, 1960]. *Brown* [1960, Table 2] reports R_1 through R_6 for 20 values of r/a between 0 and 1 that may be used for solution comparison.

The Nusselt number is defined as $Nu = hD/k$, where h is the heat transfer coefficient (a function of Re, Pr, L, and D or Q). Nu is a dimensionless temperature gradient averaged over the

tube walls and is frequently used for comparing convection solutions. For solutions where the temperature gradient is a function of location, a local Nusselt and mean Nusselt number are usually defined, where the local Nusselt number is a measure of the heat transfer at any specified location and the mean Nusselt number is a measure of the heat transfer for the whole problem domain. The local and mean Nusselt numbers $Nu_{z,T}$ and $Nu_{m,T}$ for this solution are

$$Nu_{z,T} = \frac{\sum_{n=0}^{\infty} G_n \exp\left(-2\lambda_n^2 z^*\right)}{2\sum_{n=0}^{\infty}\left(G_n/\lambda_n^2\right)\exp\left(-2\lambda_n^2 z^*\right)} \tag{A17}$$

and

$$Nu_{m,T} = \frac{1}{4z^*} ln\left(\frac{1}{\theta_m}\right) \tag{A18}$$

As a check, tabulated results for z^* versus θ_m are reported by *Shah and London* [1978; Table 13] for some of the values of z^* considered in lava tube flow. Figure A1 is a plot of this solution in dimensionless variables for use in estimating the cooling without calculating the full numeric summation of equation (A7). It can be used by determining z^* from equation (A9) or estimating it from Figure A1a. Figure A1b and the z^* value are then used to estimate the θ_m value. With this, the equation for θ_m from Table 1 and the assumed wall and entrance temperatures, the mean bulk fluid temperature for any particular tube and flow rate may be estimated. Figure A1c is the local Nusselt number versus z^* from equation (A17) and may be used for comparing the dimensionless heat out of the flow relative to other solutions.

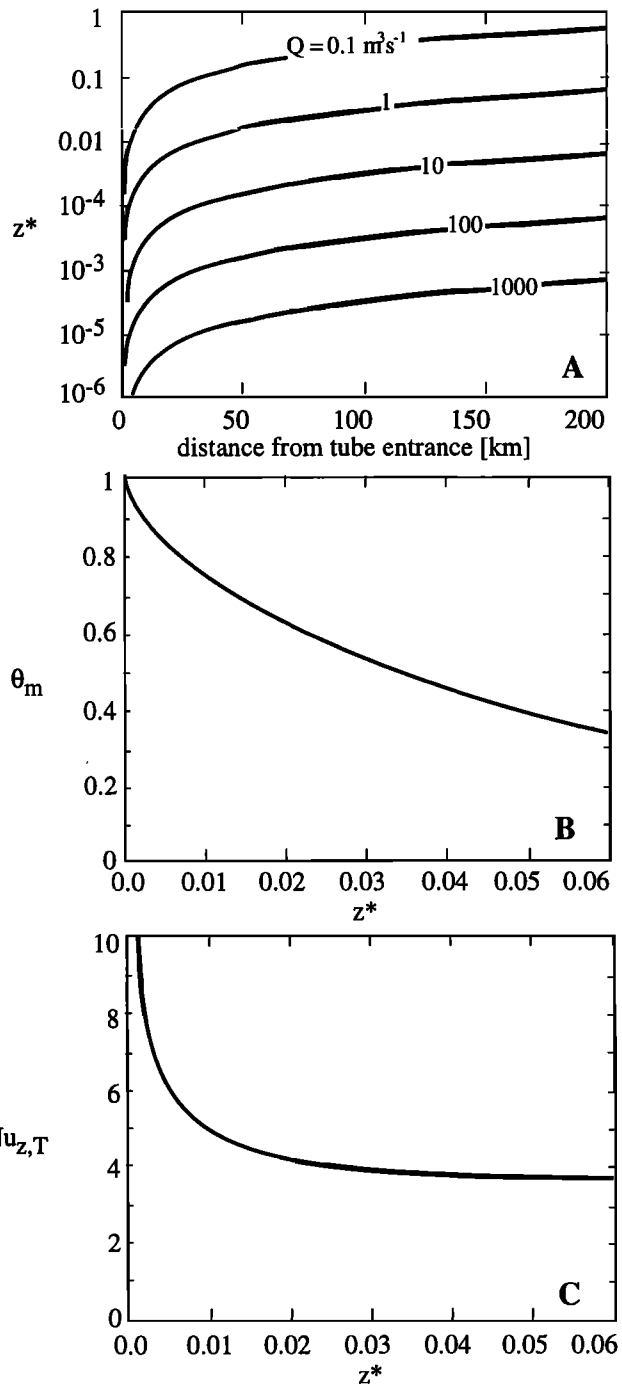

Figure A1. Graph of the constant wall temperature circular tube flow solution. (a) The dimensionless distance variable z^* as a function of distance and flow rate (ρ, k, and C_p values are given by Table 1), (b) the dimensionless bulk mean temperature θ_m as a function of the dimensionless distance, and (c) the local Nusselt number $Nu_{z,T}$ as a function of the dimensionless distance.

A2. Laminar Forced Convective Parallel Plate Flow With Constant Wall Temperature

The Grätz-Nusselt solution for the dimensionless fluid bulk mean temperature for flow between parallel plates is similar to the circular tube flow solution, but simpler. For parallel plate flow, we have [*Nusselt*, 1923; *Sellars et al.*, 1956; *Shah and London*, 1978, equations (294) through (298)] a dimensionless fluid temperature

$$\theta = \frac{T - T_w}{T_e - T_w} = \sum_{n=0}^{\infty} C_n Y_n \exp\left(-\frac{32}{3}\lambda_n^2 z^*\right), \tag{A19}$$

and a dimensionless mean bulk temperature

$$\theta_m = \frac{T_m - T_w}{T_e - T_w} = 3\sum_{n=0}^{\infty} \frac{G_n}{\lambda_n^2} \exp\left(-\frac{32}{3}\lambda_n^2 z^*\right) \tag{A20}$$

where, λ_n, Y_n, and C_n are eigenvalues, eigenfunctions, and constants, $G_n = -(C_n/2)Y_n'(1)$, and z^* is the dimensionless axial distance

$$z^* = \frac{z}{D_h Pe} = \frac{z}{D_h Re Pr}. \tag{A21}$$

For a plate separation of $2d$ and a flow width of w, $D_h = 4d$, and z^* in terms of a volume flow rate is

$$z^* = \frac{zkw}{8\rho C_p Q d}. \tag{A22}$$

The first 10 ($0 \le n \le 9$) values of λ_n and G_n are shown in Table A2 [*Brown*, 1960; *Shah and London*, 1978]. Values for the higher ($n \ge 10$) eigenvalues and constants are calculated from

$$\lambda_n = 4n + \frac{5}{3}, \quad n = 10, 11, 12\ldots \tag{A23}$$

and G_n is given by

$$G_n = 1.01278729\lambda_n^{-1/3}, \tag{A24}$$

Table A2. Parallel Plate Infinite Series Solution Functions for a Constant Wall Temperature

n	λ_n	G_n
0	1.6815953222	0.858086674
1	5.6698573459	0.569462850
2	9.6682424625	0.476065463
3	13.6676614426	0.423973730
4	17.6673735653	0.389108706
5	21.6672053243	0.363465044
6	25.6670964863	0.343475506
7	29.6670210447	0.327265745
8	33.6669660687	0.313739318
9	37.6669244563	0.302204200

Brown [1960] and *Shah and London* [1978, Table 30].

and may be used to also find C_nY_n ($G_n = -(C_n/2)Y_n'(1)$) [*Sellars et al.*, 1956; *Shah and London*, 1978, equations (297) and (298)]. Calculating Y_n for evaluating equation (A19) requires a method similar to that in the round tube constant temperature solution for R_n. Like R_n, Y_n varies with both n and y/d. It may be evaluated with the series

$$Y_n = \sum_{i=0}^{\infty} E_{ni}\left(\frac{y}{d}\right)^i \tag{A25}$$

where E_{ni} is a function of the eigenvalues (λ_n)

$$E_{ni} = 0 \quad i < 0$$

$$E_{ni} = 1 \quad i = 0 \tag{A26}$$

$$E_{ni} = -\lambda_n^2(E_{i-2} - E_{i-4})/i(i-1)$$

[*Brown*, 1960]. *Brown* [1960, Table 5] reports Y_1 through Y_6 for 20 values of y/d between 0 and 1 that may be used for solution comparison.

The local and mean Nusselt numbers $Nu_{z,T}$ and $Nu_{m,T}$ for this solution are

$$Nu_{z,T} = \frac{8}{3}\frac{\sum_{n=0}^{\infty} G_n \exp\left(-\frac{32}{3}\lambda_n^2 z^*\right)}{\sum_{n=0}^{\infty}\left(G_n/\lambda_n^2\right)\exp\left(-\frac{32}{3}\lambda_n^2 z^*\right)} \tag{A27}$$

and

$$Nu_{m,T} = \frac{1}{4z^*}\ln\left(\frac{1}{\theta_m}\right). \tag{A28}$$

As above, tabulated results of θ_m and $Nu_{z,T}$ versus z^* are reported by *Shah and London* [1978, Table 31] for solution comparisons for some of the larger values of z^* encountered in lava tubes. Figure A2a shows z^* versus z for a range of flow rates. As is indicated by equation (A22), increasing the flow width by a factor of 10 is equivalent to decreasing the flow rate by a factor of 10. Figures A2b and A2c show θ_m and $Nu_{z,T}$ versus z^* from equations (A20) and (A27), respectively. As for the tube flow solution shown in Figure A1, Figure A2 may be used in estimating the cooling without calculating the full numeric summation of equation (A20). Determine z^* from equation (A22) or estimate it from Figure A2a. Figure A2b is then used to estimate the θ_m value. With this, the equation for θ_m from Table 1 and the assumed wall and entrance temperatures, the mean bulk fluid temperature for any particular tube and flow rate may be estimated. Compare the local Nusselt numbers versus z^* in Figures A1c and A2c to see the differences in the peripheral heat losses, and note that the parallel plate solution

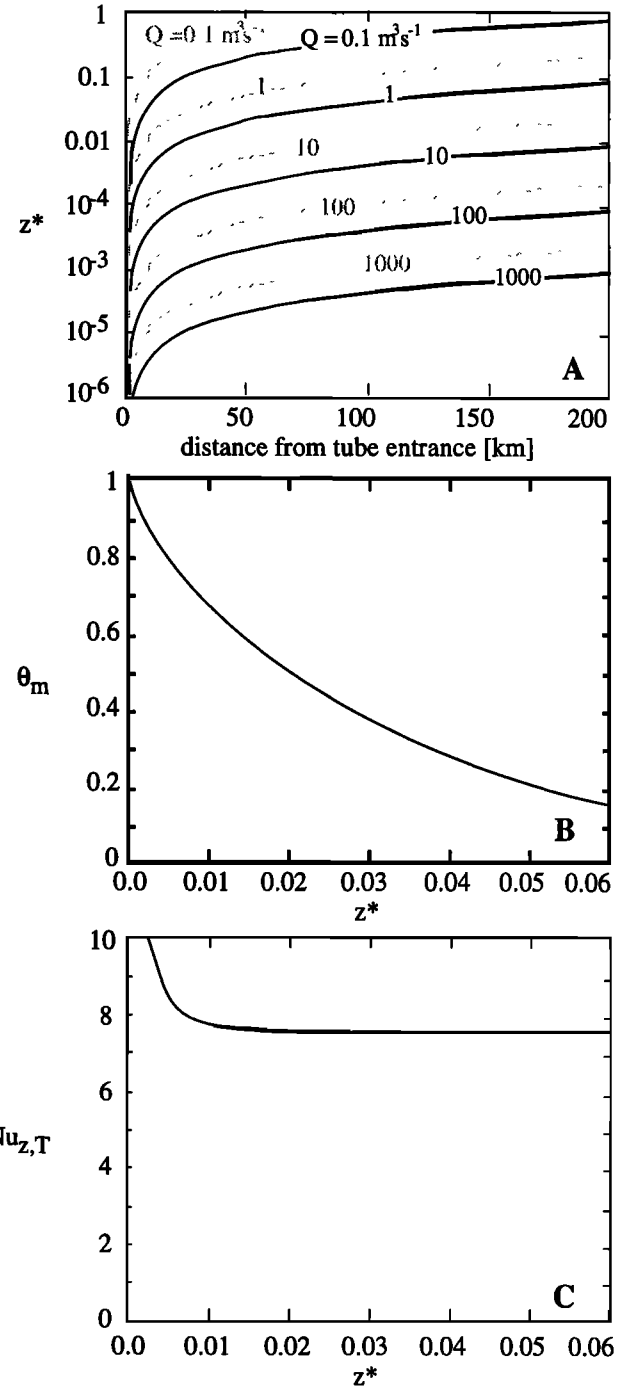

Figure A2. Graph of the constant wall temperature parallel plates flow solution. (a) The dimensionless distance variable z^* as a function of distance and flow rate (ρ, k, and C_p values from Table 1), the solid lines and flow rate contour labels are for a flow width of 5 times the plate spacing, the gray lines and flow rate contour labels are for a flow width of 12 times the plate spacing, (b) shows the dimensionless bulk mean temperature θ_m as a function of the dimensionless distance, and (c) shows the local Nusselt number $Nu_{z,T}$ as a function of the dimensionless distance.

has a higher Nusselt number for the same z^*. This is a reflection of the differences in the hydraulic diameter, or the ratio of the cross section area to the length of the perimeter losing heat. The longer perimeter of the parallel plate solution relative to the circular tube solution allows a greater loss of heat.

A3. Laminar Forced Convective Circular Tube Flow With Constant Wall Heat Flux

For the circular tube constant wall heat flux convection problem, the problem is the same as that of the circular tube with constant wall temperature except for the boundary condition

$$q_w = \text{const} \quad r = a. \tag{A29}$$

As before, we have

$$z^* = \frac{\pi}{4}\frac{zk}{\rho C_p Q} \tag{A30}$$

but here the dimensionless fluid temperature is

$$\theta = \frac{T - T_e}{(q_w D_h/k)} = 4z^* + \frac{1}{2}\left(\frac{r}{a}\right)^2 - \frac{1}{8}\left(\frac{r}{a}\right)^4 - \frac{7}{48} + \frac{1}{2}\sum_{n=1}^{\infty} C_n R_n \exp\left(-2\beta_n^2 z^*\right) \tag{A31}$$

the dimensionless mean bulk temperature is

$$\theta_m = \frac{T_m - T_e}{(q_w D_h/k)} = 4z^* \tag{A32}$$

and

$$\theta_w = \frac{T_w - T_e}{(q_w D_h/k)} = 4z^* + \frac{11}{48} + \frac{1}{2}\sum_{n=1}^{\infty} C_n R_n(1) \exp\left(-2\beta_n^2 z^*\right) \tag{A33}$$

where β_n, R_n, and C_n are eigenvalues, eigenfunctions, and constants, and equation (A33) can be used to find the wall temperature for any given flow rate [*Sellars et al.*, 1956; *Siegel et al.*, 1958]. The first 20 values for β_n^2, and $C_n R_n(1)$ are in Table A3 [*Siegel et al.*,1958; *Hsu*; 1965; *Shah and London*, 1978], and the higher (n >20) eigenvalues, functions, and constants may be calculated from [*Hsu*; 1965; *Shah and London*, 1978]

$$\beta_n = 4n + \frac{4}{3}, \quad n = 21,22,23\ldots \tag{A34}$$

and $C_n R_n$ may be calculated with

$$C_n R_n(1) = -2.401006045\beta_n^{-5/3}. \tag{A35}$$

The local Nusselt number is

$$Nu_{z,H} = \theta_w - 4z^* = +\frac{11}{48} + \frac{1}{2}\sum_{n=1}^{\infty} C_n R_n(1) \exp\left(-2\beta_n^2 z^*\right), \tag{A36}$$

and flow solutions can be checked for accuracy against the tabulation of selected values of z^* and $Nu_{z,H}$ by *Shah* [1975] and *Shah and London* [1978].

A4. Laminar Forced Convective Parallel Plate Flow With Constant Wall Heat Flux

The problem is the same as that of the parallel plate with constant wall temperature except for the boundary condition

Table A3. Circular Tube Infinite Series Solution Functions for the Constant Wall Heat Flux

n	β_n^2	$-C_n R_n(1)$
1	25.679611	0.19872216
2	83.861753	0.06925746
3	174.16674	0.03652138
4	296.53630	0.02301407
5	450.94720	0.01602945
6	637.38735	0.011906317
7	855.849532	0.009249488
8	1106.329035	0.007427222
9	1388.822594	0.006117477
10	1703.327852	0.005141193
11	2049.843045	0.004391938
12	2428.366825	0.003803024
13	2838.898142	0.003330824
14	3281.436173	0.002945767
15	3755.980271	0.002627194
16	4262.529926	0.002360296
17	4801.084.748	0.002135757
18	5371.644444	0.001940852
19	5974.208812	0.0071774030
20	6608.777727	0.001628990

Siegel et al. [1958], *Hsu* [1965], and *Shah and London* [1978, Table 17].

$$q_w = \text{const for } y = d. \tag{A37}$$

As before, we have

$$z^* = \frac{z}{D_h Pe} = \frac{z}{D_h Re Pr} = \frac{zkw}{8\rho C_p Q d} \tag{A38}$$

but here the dimensionless fluid temperature is [*Cess and Shaffer*, 1959]

$$\theta = \frac{T - T_e}{(q_w D_h/k)} = 4z^* + \frac{3}{16}\left(\frac{y}{d}\right)^2 - \frac{1}{32}\left(\frac{y}{d}\right)^4 - \frac{39}{1120} + \frac{1}{4}\sum_{n=1}^{\infty} C_n Y_n \exp\left(-\frac{32}{3}\beta_n^2 z^*\right) \tag{A39}$$

the dimensionless mean bulk temperature is

$$\theta_m = \frac{T_m - T_e}{(q_w D_h/k)} = 4z^* \tag{A40}$$

and

$$\theta_w = \frac{T_w - T_e}{(q_w D_h/k)} = 4z^* + \frac{17}{140} + \frac{1}{4}\sum_{n=1}^{\infty} C_n Y_n(1) \exp\left(-\frac{32}{3}\beta_n^2 z^*\right) \tag{A41}$$

where β_n, Y_n, and C_n are eigenvalues, eigenfunctions, and constants, and equation (A37) can be used to find the wall temperature for any given flow rate. The first 10 values for β_n, and $C_n Y_n$ are in Table A4 [*Cess and Shaffer*, 1959; *Sparrow et al.*, 1963; *Shah and London*, 1978] The higher (n >10) eigenvalues, functions, and constants may be calculated from [*Cess and Shaffer*, 1959; *Shah and London*, 1978]

$$\beta_n = 4n + \frac{1}{3}, \quad n = 11,12,13\ldots \tag{A42}$$

and

$$C_n Y_n(1) = -2.401006045\beta_n^{-5/3}. \tag{A43}$$

Table A4. Parallel Plate Infinite Series Solution Functions for the Constant Wall Heat Flux

n	β_n^2	$-C_nY_n(1)$
1	4.287224	0.2222280
2	8.30372	0.0725316
3	12.3106	0.0373691
4	16.3145	0.0232829
5	20.3171	0.0161112
6	24.3189	0.0119190
7	28.3203	0.0092342
8	32.3214	0.0074013
9	36.3223	0.0060881
10	40.3231	0.0051116

Sparrow et al. [1963] and *Shah and London* [1978, Table 33].

The local Nusselt number is

$$Nu_{z,H} = \theta_w - 4z^* = \frac{17}{140} + \frac{1}{4}\sum_{n=1}^{\infty} C_n Y_n(1) exp\left(-\frac{32}{3}\beta_n^2 z^*\right), \quad (A44)$$

and flow solutions can be checked for accuracy against the tabulation of selected values of z^* and $Nu_{z,H}$ by *Shah* [1975] and *Shah and London* [1978].

Acknowledgments. This research was performed while S.S. held a National Research Council Resident Research Associateship at NASA's Goddard Space Flight Center. Portions of the Alba Patera lava tube analysis conducted by S.S. were supported by a NASA Planetary Geology and Geophysics Program Grant. Contributions by M.Z. were supported by a grant from the NASA Planetary Geology and Geophysics Program. We thank H. Pinkerton, L. Wilson, and S. Blake for constructive and thorough reviews that significantly improved the clarity of the manuscript; L. Keszthelyi for numerous lava tube discussions, and especially K.V. Cashman, C. Thornber, and P.J. Stephenson for lava tube temperature and crystallinity data and discussions.

References

Atkinson, A., and V. Atkinson, Undara Volcano and its lava tubes, 86 pp., A. and V. Atkinson, Ravenshoe, Australia, 1995.

Atkinson, A., T.J. Griffin, and P.J. Stephenson, A major lava tube system from Undara Volcano, North Queensland, *Bull. Volcanol., 39*, 266-293, 1975.

Baldridge, W.S., Lucero, New Mexico, in *Volcanoes of North America: United States and Canada*, edited by C.A. Wood and J. Kienle, pp. 305-306, Cambridge Univ. Press, New York, 1990.

Bhattacharyya, T.K., and D.N. Roy, Laminar heat transfer in a round tube with variable circumferential or arbitrary wall heat flux, *Int. J. Heat Mass Transfer, 13*, 1057-1060, 1970.

Bird, R.B., W.E. Stewart, and E.N. Lightfoot, *Transport Phenomena*, 780 pp., John Wiley, New York, 1960.

Bird, R.B., R.C. Armstrong, and O. Hassager, *Dynamics of Polymeric Liquids*, 649 pp., John Wiley, New York, 1987.

Brown, G.M., Heat or mass transfer in a fluid in laminar flow in a circular or flat conduit, *AIChE J., 6*, 179-183, 1960.

Burmeister, L.C., *Convective Heat Transfer*, 2nd ed., John Wiley, New York, 1993.

Carr, M.H., *The Surface of Mars*, 232 pp., Yale Univ. Press, New Haven, Conn., 1981.

Carr, M.H., R. Greeley, K.R. Blasius, J.E. Guest, and J.B. Murray, Some Martian volcanic features as viewed from the Viking orbiters, *J. Geophys. Res., 82*, 3985-4015, 1977.

Cashman, K.V., J.P. Kauahikaua, and J.E. Pallon, Vesicle structure of inflated sheet flows, Kilauea and Mauna Loa volcanoes, Hawaii, *Eos Trans., 74 (43)*, Fall Meet. Suppl., 640-641, 1993.

Cashman, K.V., M.T. Mangan, and S. Newman, Surface degassing and modifications to vesicle size distributions in active basalt flows, *J. Volcanol. Geotherm. Res., 61*, 45-68, 1994.

Cattermole, P., Sequence, rheological properties, and effusion rates of volcanic flows at Alba Patera, Mars, *Proc. Lunar Planet. Sci. Conf.*, Part 2, *J. Geophys. Res., 92*, suppl., E553-E560, 1987.

Cattermole, P., Volcanic development at Alba Patera, Mars, *Icarus, 83*, 453-493, 1990.

Cess, R.D., and E.C. Shaffer, Heat transfer to laminar flow between parallel plates with a prescribed wall heat flux, *Appl. Sci. Res. A, 8*, 339-344, 1959.

Chow, V.T., *Open-Channel Hydraulics*, 680 pp., McGraw-Hill, New York, 1959.

Crisp, J., S.E.H. Sakimoto, and S.M. Baloga, , Lava tube pressure and gravity driving forces: constraints on tube lengths, flow rates and surface breakout locations, *Eos Trans. AGU, 76 (46)*, Fall Meet. Suppl., F667, 1995.

Donnelly-Nolan, J.M., Medicine Lake Volcano and Lava Beds National Monument, *Calif. Geol., 20*, 145-153, 1992.

Eckert, E.R.G., and R.M. Drake Jr., *Analysis of Heat and Mass Transfer*, 806 pp., Hemisphere, New York, 1987.

Glaze, L.S., G.N. Karas, S.I. Chernobieff, M.W. Thomas, E.D. Paylor, and D.C. Pieri, Kilauea: Compiled volcanology data, set 1, Jet Propul. Lab., Pasadena, Calif., 1992.

Grätz, L., Über die Wärmeleitungs fähigkeit von Flüssigkeiten, *Ann. der Phys. and Chem., 18*, 79-94, 1883.

Greeley, R., Basaltic "plains" volcanism, in *Volcanism of the Eastern Snake River Plain, Idaho: A Comparative Planetary Geology Guidebook*, edited by R. Greeley and J.S. King, NASA Conf. Rep. CR-154621, 23-44, 1977.

Greeley, R., The Snake River Plain, Idaho: Representative of a new category of volcanism, *J. Geophys. Res., 87*, 2705-2712, 1982.

Greeley , R., The role of lava tubes in Hawaiian volcanoes, in *Volcanism in Hawaii*, edited by R.W. Decker, T.L. Wright, and P.H. Stauffer, *U.S. Geol. Surv. Prof. Pap. 1350*, 1569-1588, 1987.

Hammond, P., Indian Heaven, Washington, in *Volcanoes of North America: United States and Canada*, edited by C.A. Wood, and J. Kienle, pp. 166-167, Cambridge Univ. Press, New York, 1990.

Hardee, H.C., Heat transfer measurements of the 1983 Kilauea lava flow, *Science, 222*, 47-48, 1983.

Hardee, H.C., Convection heat transfer rates in molten lava, in *Active Lavas: Monitoring and Modelling*, edited by C.J. Kilburn and G. Luongo, pp. 193-201, UCL Press, London, 1993.

Head, J.W., L.S. Crumpler, J.C. Abule, J.E. Guest, and R.S. Saunders, Venus volcanism: Classification of volcanic features and structures, associations, and global distribution from Magellan data, *J. Geophys. Res., 97*, 13,153-13,197, 1992.

Heliker, C., and T.L. Wright, The Pu'u O'o-Kupaianaha eruption of Kilauea, *Eos Trans. AGU, 72*, 521, 526, 530, 1991.

Helz, R.T., and C.R. Thornber, Geothermometry of Kilauea Iki lava lake, Hawaii, *Bull. Volcanol., 49*, 651-668, 1987.

Helz, R.T., C. Heliker, M. Mangan, K. Hon, C.A. Neal, and L. Simmons, Thermal history of the current Kilauean East Rift eruption, *Eos Trans. AGU, 71(44)*, Fall Meeting Suppl., 557-558, 1991.

Helz, R.T., N.G. Banks, C. Heliker, C.A. Neal, and E.W. Wolfe, Comparative geothermometry of recent Hawaiian eruptions, *J. Geophys. Res., 100*, 17637-17657, 1995.

Ho, A.M., and K.V. Cashman, Temperature constraints on the Ginkgo flow of the Columbia River Basalt Group, *Geology, 25* (5), 403-406, 1997.

Hodges, C.A., and H.J. Moore, Atlas of volcanic landforms on Mars, *U.S. Geol. Surv. Prof. Pap., 1534*, 194pp., 1992.

Holcomb, R.T., Eruptive history and long-term behavior of Kilauea Volcano, in *Volcanism in Hawaii*, edited by R.W. Decker, T.L. Wright, and P.H. Stauffer, *U.S. Geol. Surv. Prof. Pap., 1350*, 261-350, 1987.

Hon, K., J. Kauahikaua, R. Denlinger, and K. Mackay, Emplacement and inflation of pahoehoe sheet flows: Observations and measurements of active lava flows on Kilauea Volcano, Hawaii, *Geol. Soc. Am. Bull., 106*, 351-370, 1994.

Hsu, C.J., Heat transfer in a round tube with sinusoidal wall heat flux distribution, *AIChE J., 11*, 690-695, 1965.

Incropera, F.P., and D.P. DeWitt, *Fundamentals of Heat and Mass Transfer*, 886 pp., John Wiley, New York, 1996.

Kakaç, S., and Y. Yener, *Convective Heat Transfer*, 2nd ed., 422 pp., CRC Press, Boca Raton, Fla., 1995.

Kauahikaua, J., Observations on basaltic lava stream dynamics in tubes from Kilauea, Hawai'i, in *AGU Chapman Conference on Long Lava Flows*, edited by P.J. Stephenson and P.W. Whitehead, pp. 32-33, James Cook University of North Queensland, Townsville, Australia, 1996.

Kauahikaua, J., M. Mangan, C. Heliker, and T. Mattox, The death of Kupaianaha vent, Kilauea volcano, Hawaii, *Eos Trans. AGU, 73(43)*, Fall Meeting Suppl., 629, 1992.

Kauahikaua, J., M. Mangan, C. Heliker, and T. Mattox, A quantitative look at the demise of a basaltic vent: The death of Kupaianaha, Kilauea Volcano, Hawai'i, *Bull. Volcanol., 57*, 641-648, 1996.

Keszthelyi, L., A preliminary thermal budget for lava tubes on the Earth and planets, *J. Geophys. Res., 100*, 20411-20420, 1995.

Kuntz, M.A., D.E. Champion, E.C. Spiker, R.H. Lefebvre, and L.A. McBroome, The Great Rift and the evolution of the Craters of the Moon lava field, Idaho, in *Cenozoic Geology of Idaho*, edited by B. Bonnichsen, and R.M. Breckenridge, *Bull. Idaho Bur. Mines Geol., 26*, 423-437, 1982.

Kuntz, M.A., H.R. Covington, and L.J. Schorr, An overview of the basaltic volcanism of the eastern Snake River Plain, Idaho, in *Regional Geology of Eastern Idaho and Western Wyoming*, edited by P.K. Link, M.A. Kuntz, and L.B. Platt, *Geo. Soc. Am. Mem., 179*, 227-267, 1992.

Malin, M.C., Lengths of Hawaiian lava flows, *Geology, 8*, 306-308, 1980.

Mangan, M.T., C.C. Heliker, T.N. Mattox, J.P. Kauahikaua, and R.T. Helz, Episode 49 of the Pu'u O'o-Kupaianaha eruption of Kilauea Volcano-breakdown of a steady-state eruptive era, *Bull. Volcanol., 57*, 127-135, 1995.

Marsh, B.D., On the crystallinity, probability of occurrence, and rheology of lava and magma, *Contrib. Mineral. Petrol., 78*, 85-98, 1981.

Mattox, T.N., C. Heliker, J. Kauahikaua, and K. Hon, Development of the 1990 Kalapana Flow Field, Kilauea Volcano, Hawaii, *Bull. Volcanol., 55*, 407-413, 1993.

Mouginis-Mark, P.J., L. Wilson, and J.R. Zimbelman, Polygenic eruptions on Alba Patera, Mars, *Bull. Volcanol., 50*, 361-379, 1988.

Nusselt, W., Der Wärmeaustausch am Berieselungskühler, *VDI Z., 67*, 206-210, 1923.

Peterson, D.W., R.T. Holcomb, R.I. Tilling, and R.L. Christiansen, Development of lava tubes in the light of observations at Mauna Ulu, Kilauea Volcano, Hawaii, *Bull. Volcanol., 56*, 343-360, 1994.

Realmuto, V.J., K. Hon, A.B. Kahle, E.A. Abbott, and D. Pieri, Multispectral thermal infrared mapping of the 1 October 1988 Kupaianaha flow field, Kilauea volcano, Hawaii, *Bull. Volcanol., 55*, 33-44, 1992.

Sakimoto, S.E.H., Problems in physical volcanology: Analytic and computational models of buoyant diapir ascent, variable viscosity dome emplacement, and non-Newtonian lava tube flow, Ph.D. thesis, 97 pp., Johns Hopkins Univ., Baltimore, Md., 1995a.

Sakimoto, S.E.H., A temperature dependent power law rheology from field and laboratory data for cooling basaltic lava flow models, *Eos Trans. AGU, 76* (46), Fall Meet. Suppl., 650, 1995b.

Sakimoto, S.E.H., and M.T. Zuber, Lava tube flow: The influence of tube geometry, non-Newtonian rheology, and thermal boundary conditions on predicted cooling, in *Chapman Conference on Long Lava Flows: Conference Abstracts Long Lava Flows, Econ Geol. Res. Unit Contrib. 56*, edited by P.W. Whitehead, pp. 66-67, Dep. of Earth Sci., James Cook Univ. of N. Queensl., Townsville, Australia, 1996.

Sakimoto, S. E. H., J. Crisp, and S.M. Baloga, Eruption constraints on tube-fed planetary lava flows, *J. Geophys. Res., 102*, 6597-6613, 1997.

Schneeberger, D.M., and D.C. Pieri, Geomorphology and stratigraphy of Alba Patera, Mars, *J. Geophys. Res., 96*, 1907-1930, 1991.

Self, S., T. Thordarson, L. Keszthelyi, G.P.L. Walker, K. Hon, M.T. Murphy, P. Long, and S. Finnemore, A new model for the emplacement of Columbia River basalts as large, inflated pahoehoe lava flow fields, *Geophys. Res. Lett., 23*, 2689-2692, 1996.

Sellars, J.R., M. Tribus, and J.S. Klein, Heat Transfer to laminar flow in a round tube or flat conduit: The Grätz problem extended, *Trans. ASME, 78*, 441-448, 1956.

Shah, R.K., Thermal entry length solutions for the circular tube and parallel plates, in *Proceedings of 3rd National Heat and Mass Transfer Conference*, vol. I, paper HMT-11-75, Indian Inst. Technol., Bombay, 1975.

Shah, R.K., and A.L. London, *Laminar Flow Forced Convection in Ducts*, 477 pp., Academic, San Diego, Calif., 1978.

Shaw, H.R., Rheology of basalt in the melting range, *J. Petrol., 10*, 510-535, 1969.

Shaw, H.R., T.L. Wright, D.L. Peck, and R. Okamura, The viscosity of basaltic magma: An analysis of field measurements in Makaopuhi lava lake, Hawaii, *Am. J. Sci., 266* , 225-264, 1968.

Siegel, R., E.M. Sparrow, and T.M. Hallman, Steady laminar heat transfer in a circular tube with prescribed wall heat flux, *Appl. Sci. Res.*, Ser. # *A, 7*, 386-392, 1958.

Skelland, A.H.P., *Non-Newtonian Flow and Heat Transfer*, 469 pp., John Wiley, New York, 1967.

Sparrow, E.M., J.L. Novotny, and S.H. Lin, Laminar heat flow of a heat-generating fluid in a parallel-plate channel, *AIChE J., 9*, 797-804, 1963.

Stephenson, P.J., Ridges and depressions in the Undara lava flow, N. Qld: Alternative mechanisms for their formation, in *Chapman Conference on Long Lava Flows: Conference Abstracts Long Lava Flows, Econ Geol. Res. Unit Contrib. 56*, edited by P.W. Whitehead, pp. 82-83, Dep. of Earth Sci., James Cook Univ. of N. Queensl., Townsville, Australia, 1996.

Stephenson, P.J., and T.J. Griffin, Some long basaltic lava flows in North Queensland, in *Volcanism in Australasia*, edited by R.W. Johnson, pp. 41-51, Elsevier, New York, 1976.

Stephenson, P.J., and P.W. Whitehead, Lava pits in the Toomba basalt, in *Chapman Conference on Long Lava Flows: Conference Abstracts Long Lava Flows, Econ Geol. Res. Unit Contrib. 56*, edited by P.W. Whitehead, pp. 80-81, Dep. of Earth Sci., James Cook Univ. of N. Queensl., Townsville, Australia, 1996.

Stephenson, P.J., T.J. Griffin, and F.L. Sutherland, Cainozoic volcanism in Northeastern Australia, in *The Geology and Geophysics of Northeastern Australia*, edited by R.A. Henderson, and P.J. Stephenson, pp. 349-374, Geol. Soc. of Aust., Queensland Div., Brisbane, 1980.

Stephenson, P.J., A.T. Burch-Johnson, and D. Stanton, Long lava flows in North Queensland–Context, characteristics, emplacement, in *Chapman Conference on Long Lava Flows: Conference Abstracts Long Lava Flows, Econ Geol. Res. Unit Contrib. 56*, edited by P.W. Whitehead, pp. 86-87, Dep. of Earth Sci., James Cook Univ. of N. Queensl., Townsville, Australia, 1996.

Swanson, D.A., Pahoehoe flows from the 1969-1971 Mauna Ulu eruption, Kilauea Volcano, Hawaii, *Geol. Soc. Am. Bull., 84*, 615-626, 1973.

Swanson, D.A., and P.B. Fabbi, Loss of volatiles during fountaining and flowage of basaltic lava at Kilauea Volcano, Hawaii, *J. Res. U.S. Geol. Surv., 1*, 649-658, 1973.

Theilig, E., Zuni-Bandera, New Mexico, in *Volcanoes of North America: United States and Canada*, edited by C.A. Wood and J. Kienle, pp. 303-305, Cambridge Univ. Press, New York, 1990a.

Theilig, E., Carrizozo, New Mexico, in *Volcanoes of North America: United States and Canada*, edited by C.A. Wood and J. Kienle, pp. 308-309, Cambridge Univ. Press, New York, 1990b.

U.S. Geological Survey, Hawaii Volcanoes National Park and vicinity, Hawaii, USGS 1:100,000 scale topographic map, Hawaii Volcanoes National Park, 1986.

Waters, A.C., J.M. Donnelly-Nolan, and B.W. Rogers, Selected caves and lava-tube systems in and near Lava Beds National Monument, California, *U.S. Geol. Surv. Bull., 1673*, 102pp., 1990.

White, F.M., *Viscous Fluid Flow*, 614 pp., McGraw-Hill, New York, 1991.

Whitehead, P.W., and P.J. Stephenson, Lava rise ridges of the Toomba basalt flow, North Queensland, in *Chapman Conference on Long Lava Flows: Conference Abstracts Long Lava Flows, Econ Geol. Res. Unit Contrib. 56*, edited by P.W. Whitehead, pp. 94-95, Dep. of Earth Sci., James Cook Univ. of N. Queensl., Townsville, Australia, 1996.

Whitehead, P.W., and P.J. Stephenson, Lava rise ridges of the Toomba basalt flow, North Queensland, Australia, *J. Geophys. Res.*, this issue.

Wolfe, E.W., M.O. Garcia, D.B. Jackson, R.Y. Koyanagi, C.A. Neal, and A.T. Okamura, The Pu'u O'o eruption of Kilauea Volcano, episodes 1-20, January 3, 193, to June 8, 1984, *U.S. Geol. Surv. Prof. Pap., 1463*, 1-98, 1987.

Zebker, H.A., P. Rosen, S. Hensley, and P.J. Mouginis-Mark, Analysis of active lava flows on Kilauea volcano, Hawaii, using SIR-C radar correlation measurements, *Geology, 24*, 495-498, 1996.

S.E.H. Sakimoto, Geodynamics Branch, Code 921, NASA/Goddard Space Flight Center, Greenbelt, MD 20771. (e-mail: sakimoto@denali.gsfc.nasa.gov).

M.T. Zuber, Department of Earth, Atmospheric and Planetary Sciences, 54-518, Massachusetts Institute of Technology, Cambridge, MA 02139. (e-mail: zuber@tharsis.gsfc.nasa.gov).

(Received May 13, 1997; revised October 2, 1997;
accepted October 27, 1997)